Article

Development of High-Resolution Soil Hydraulic Parameters with Use of Earth Observations for Enhancing Root Zone Soil Moisture Product

Juby Thomas [1], Manika Gupta [1,*], Prashant K. Srivastava [2], Dharmendra K. Pandey [3] and Rajat Bindlish [4]

[1] Department of Geology, University of Delhi, Delhi 110007, India
[2] Remote Sensing Laboratory, Institute of Environment and Sustainable Development, Banaras Hindu University, Varanasi 221005, India
[3] Space Applications Centre—ISRO, Ahmedabad 380015, India
[4] Hydrological Sciences Laboratory, NASA Goddard Space Flight Centre, Greenbelt, MD 20771, USA
* Correspondence: manikagup@gmail.com

Abstract: Regional quantification of energy and water balance fluxes depends inevitably on the estimation of surface and rootzone soil moisture. The simulation of soil moisture depends on the soil retention characteristics, which are difficult to estimate at a regional scale. Thus, the present study proposes a new method to estimate high-resolution Soil Hydraulic Parameters (SHPs) which in turn help to provide high-resolution (spatial and temporal) rootzone soil moisture (RZSM) products. The study is divided into three phases—(I) involves the estimation of finer surface soil moisture (1 km) from the coarse resolution satellite soil moisture. The algorithm utilizes MODIS 1 km Land Surface Temperature (LST) and 1 km Normalized difference vegetation Index (NDVI) for downscaling 25 km C-band derived soil moisture from AMSR-2 to 1 km surface soil moisture product. At one of the test sites, soil moisture is continuously monitored at 5, 20, and 50 cm depth, while at 44 test sites data were collected randomly for validation. The temporal and spatial correlation for the downscaled product was 70% and 83%, respectively. (II) In the second phase, downscaled soil moisture product is utilized to inversely estimate the SHPs for the van Genuchten model (1980) at 1 km resolution. The numerical experiments were conducted to understand the impact of homogeneous SHPs as compared to the three-layered parameterization of the soil profile. It was seen that the SHPs estimated using the downscaled soil moisture (*I-d* experiment) performed with similar efficiency as compared to SHPs estimated from the in-situ soil moisture data (*I-b* experiment) in simulating the soil moisture. The normalized root mean square error (nRMSE) for the two treatments was 0.37 and 0.34, respectively. It was also noted that nRMSE for the treatment with the utilization of default SHPs (*I-a*) and AMSR-2 soil moisture (*I-c*) were found to be 0.50 and 0.43, respectively. (III) Finally, the derived SHPs were used to simulate both surface soil moisture and RZSM. The final product, RZSM which is the daily 1 km product also showed a nearly 80% correlation at the test site. The estimated SHPs are seen to improve the mean NSE from 0.10 (*I-a* experiment) to 0.50 (*I-d* experiment) for the surface soil moisture simulation. The mean nRMSE for the same was found to improve from 0.50 to 0.31.

Keywords: soil moisture downscaling; root zone soil moisture; soil hydraulic parameters; HYDRUS-1D; AMSR-2; MODIS

1. Introduction

Soil moisture is one of the most critical environmental variables for understanding energy and water balance, both regionally and locally [1]. It controls the interchange of energy and water fluxes at the interface of the atmosphere and land surface [2]. Soil moisture plays a pivotal role in various earth system processes such as precipitation's partitioning into surface runoff and infiltration and partitioning of solar radiation into latent heat, sensible heat, and ground heat fluxes [3]. In the current scenario of increased

number of extreme climatic events, acquiring high-resolution surface and root zone soil moisture (RZSM) data is crucial for quantifying energy, water and mass exchange [4]. Additionally, it has a direct role in the domain of agriculture, irrigation, biodiversity, terrain management and trafficability, and weather and climate forecasting [5–8]. Being a causative factor, it has a further role in adverse events such as drought, floods, and geohazards such as landslides and debris flows [9–14].

Although, soil moisture is an important state variable that varies horizontally and vertically over time, estimating the same still remains challenging primarily because of terrain heterogeneity [15], inaccessibility of the terrain, huge cost of establishing and maintaining closely spaced soil moisture observational networks [16,17]. A number of ground-based, in-situ, techniques have been developed to measure soil moisture at a point scale [2]. However, the in-situ measured soil moisture cannot be utilized in estimating the same at a regional or global scale due to high variability [2].

Remotely sensed data are the most appropriate solution to acquire soil moisture data at a large areal extent. Satellite remote sensing with the help of passive and active microwave sensors can provide soil moisture data covering the entire globe [18]. Since microwave wavelengths can penetrate clouds, microwave sensors can obtain data throughout the day, regardless of the lighting conditions. A number of passive as well as active microwave sensors/missions are being recently utilized for collecting soil moisture globally, including Advanced Microwave Scanning Radiometer-2 (AMSR-2), Advanced Microwave Scanning Radiometer E (AMSR-E), Soil Moisture and Ocean Salinity (SMOS), and Soil Moisture Active Passive (SMAP) mission, and Advanced Scatterometer (ASCAT). Even though active microwave sensors provide data at a high resolution, it is achieved at the expense of low temporal resolution because of the narrow swath. On the other hand, passive microwave sensors (radiometers) require a very large aperture to detect low levels of naturally emitted microwave radiation from the objects or surface of the earth [18]. Most of the passive microwave radiometer sensors have a spatial resolution varying between 25 and 40 km, which is considered coarse, especially for agricultural studies [19]. Thus, due to the instrument's coarse spatial resolution, the retrieved satellite soil moisture also has a coarser spatial resolution. However, with data fusion techniques, the merging of SMAP and Sentinel-1 provides surface soil moisture data at a spatial resolution of 3 km [20]. These satellite sensors retrieve data for a depth of 0–5 cm only [21].

The present study puts forward a method to simulate the daily 1 km RZSM and is carried out in three phases. The soil moisture simulation depends on soil retention characteristics, which are difficult to estimate on a regional scale. Most of the studies utilize literature-based values that are dependent on the soil texture of the study area or are estimated using the pedotransfer functions [22]. However, one needs to be careful in utilizing these values as the retention characteristics of soil may change with time depending on the process the soil may undergo such as agricultural activities and weathering. These processes tend to change the porosity of the soil. Thus, to improve the soil moisture simulation, it is necessary to first estimate these retention characteristics of the soil. In the current, study, a method is presented to first derive these properties. It is hypothesized that the soil moisture-based Earth observations provide information that can be inversely utilized to estimate the soil properties. However, as mentioned earlier the microwave data are coarse resolution; we first downscale the microwave soil moisture, to include the spatial heterogeneity of the region. So, the new algorithm utilizes the Earth observations with a numerical model to estimate the soil properties that are the effective Soil Hydraulic Parameters (SHPs). Thus, the first phase uses a modified algorithm to downscale 25 km AMSR-2 soil moisture to 1 km resolution. Here, the AMSR-2 C-band data have been used as long-term data are available with AMSR-E data starting in 2002. This dataset gives an opportunity to develop a long-term soil moisture dataset compared to L-Band data such as SMAP, which is a recent dataset. Additionally, in another study, the performance of the AMSR-2 C-band and LPRM datasets was found to be similar to the SMAP dataset in the Central Ganges plain [23]. A number of approaches have been used by various researchers

to disaggregate the coarser resolution soil moisture to finer resolution. Soil evaporative efficiency and soil moisture [24], LST, NDVI, and soil moisture [25], MODIS and physical based Soil Evaporative Efficiency (SEE) model [1,26], Evaporative Fraction (EF) and Actual Evaporative Fraction (AEF) [27], Sequential model [28], Disaggregation based on Physical And Theoretical scale Change (DisPATCh) algorithm [28], Enhanced Vegetation Index (EVI) and surface temperature from MODIS are some of the popular disaggregation methods. Most of these algorithms are knitted by utilizing the relationship among finer LST, VI, and coarser soil moisture. Considering the available approaches, we have utilized LST, NDVI and AMSR-2 C-band derived soil moisture [1]. In the second phase, the downscaled soil moisture is utilized in inversely deriving the SHPs required for the simulation of soil water content in HYDRUS-1D [29]. The consistency of SHPs is evaluated based on the numerical experiments considered in the present study. In the third phase of the study, the optimized SHPs based on downscaled soil moisture are utilized to model the soil moisture content in the unsaturated zone and provide RZSM at a 1 km spatial resolution with a daily temporal resolution. The importance of the study lies in the fact that the algorithm proposed in this study is intended to make it independent of in-situ data. This method would be helpful for the unmonitored regions and this method is replicable globally wherever the satellite data products are available.

The study presented in this paper is organized as follows. Section 2 briefly describes the satellite and ground-based observations and the equipment used to monitor the soil moisture at validation sites. Section 3 outlines the soil moisture downscaling algorithm, and numerical simulations to optimize SHPs and derive RZSM. Results are discussed in detail in Section 4 followed by discussion in Section 5. Section 6 includes the conclusions and limitations of the present study.

Study Area

The validation sites are located in the agricultural belt of Northern India, in the Varanasi district of Uttar Pradesh, India. The latitudinal and longitudinal extent of the district is 25.17°N–25.58°N and 82.66°E–83.19°E, respectively. Figure 1 shows the geographical location of the study area. The region experiences a humid sub-tropic climate, Cwa or Cwb according to Köppen–Geiger climate classification [30]. The region experiences warm summers with temperatures often going above 40 °C and mild dry winters with temperatures going as low as 2 °C because of the cold waves from the Himalayas [31]. The study area receives an average annual rainfall of 103.6 cm and the majority of the rainfall events happen between June and September. The total areal extent of the district is 1535 km^2 and the total population is 3.68 million as per the 2011 census of India. The area has a high population density [32]. The study area (Figure 1) can be characterized by quaternary alluvium deposits with younger and older alluvium. The rich soil in the study area is formed and frequently enriched by erosional and depositional activities of the river Ganges, its tributaries, and channels. Geomorphologically the region can be broadly classified into active flood plains of the river Ganges and its tributaries, and older flood plains of the same. The distribution of the elevation over the study area is given in Figure 1 (C) and it shows that the majority of the area has an elevation range of 60 to 100 m above Mean Sea Level (MSL) with maximum elevation reaching less than 200 m above MSL [33]. The land use of the study area is dominated by agricultural activities and small-scale farmers hold the majority of the agricultural land.
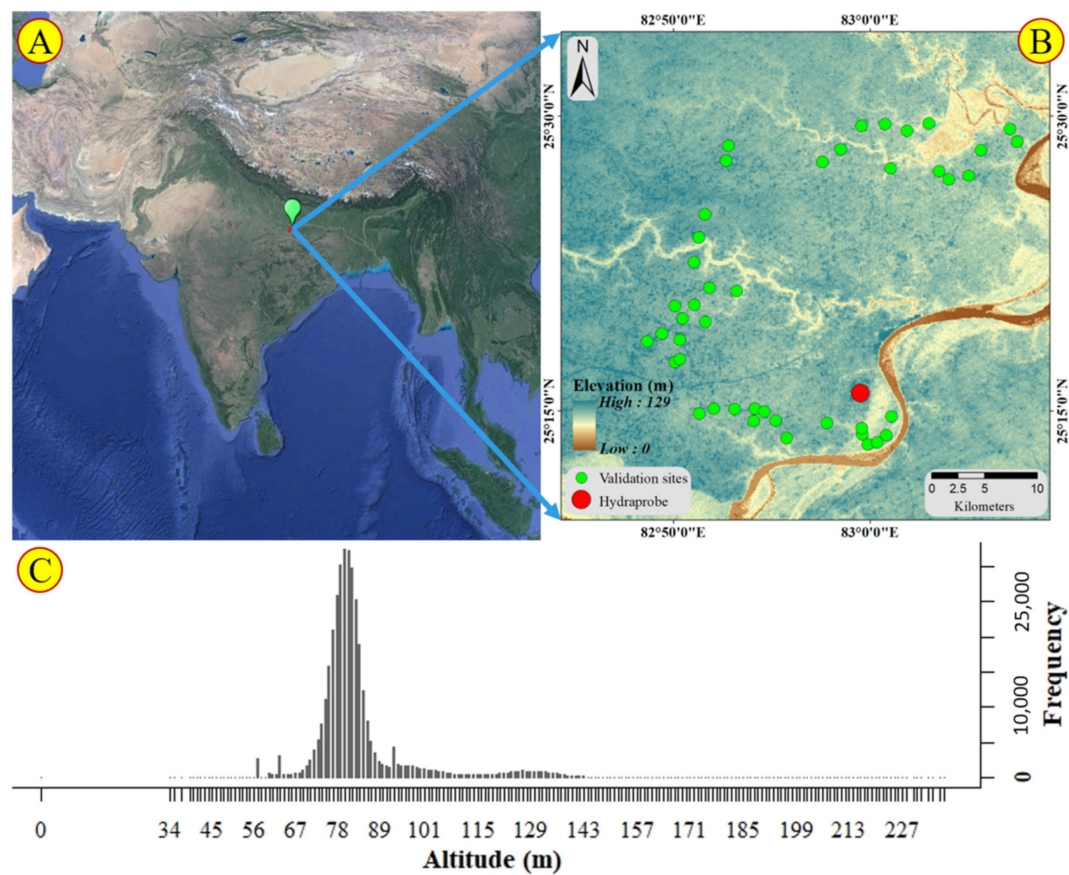
Figure 1. (**A**) Geographical location of the study area in the Indian sub-continent. (**B**) Geographical extent of the study area along with spatial distribution of validation sites and the location of HydraProbe at the validation site. Red dot represents the HydraProbe site, where Stevens HydraProbe soil moisture sensor is permanently installed. Green dots represent the 44 validation sites, where surface soil moisture is obtained for six random days during the study through gravimetric analysis. (**C**) Distribution of altitude in the study area from MSL.

2. Data Sources

The study region has comparatively homogeneous soil types and agricultural areas. This section discusses the collection of in-situ soil moisture data and satellite-derived datasets that were used for the present study. Satellite data sets used in this study for the development of the model are freely available and sources are mentioned in the data availability statement.

2.1. In-Situ Soil Moisture Data

The soil moisture sensor, Stevens HydraProbe, is installed at a site (calibration and validation site for Scatsat-1 and NASA—ISRO Synthetic Aperture Radar (NISAR)), located at Institute of Environment and Sustainable Development, Banaras Hindu University, Varanasi where soil moisture is being monitored continuously at 5 cm, 20 cm, and 50 cm depth since 2017 at hourly intervals. Stevens HydraProbe is a reliable resource for measuring soil moisture and other parameters such as soil temperature and precipitation and has been extensively used in similar studies [34–36]. The surface soil moisture data are also validated spatially at 44 different sites where in-situ measured surface soil moisture data were available on six dates: 1 January 2018, 5 February 2018, 16 February 2018, 28 March 2018, 18 April 2018 and 4 June 2018 (Figure 1). Three surface soil samples were collected at each site on each sampling date. Thus, 24 samples were collected in total at each of the 44 sites. The analysis was carried out using the gravimetric method, where the soil samples were oven dried and the difference in weight of wet soil and oven-dried soil

was taken as the moisture content of the soil. For the second phase of the study, six-month in-situ soil moisture data from the HydraProbe site from January to June 2018, has been utilized to obtain the SHPs. The October–December 2018 in-situ soil moisture data are used for validating the simulated soil moisture with the utilization of estimated SHPs. The period July to September 2018 is the Monsoon period and the soil is usually saturated due to which in-situ soil moisture was not available at the HydraProbe site.

2.2. MODIS Data

The current study utilizes the Moderate Resolution Imaging Spectroradiometer's (MODIS) daily (day and night) Land Surface Temperature (LST) version 6 (MOD11A1. 006) having a spatial resolution of 1 km [37]. Along with MOD11A1. 006, products of MOD13A2.006 are used for establishing coefficients of regression and fractional vegetation index in the algorithm [38]; 16 days NDVI, 16 days VI Quality indicators, and 16 days composite day of the year are the data set layers that are used from MOD13A2.006. The Vegetation Indices (VI) are derived from the combination of multiple bands. In the current study, the Normalized Difference Vegetation Index (NDVI) is used, which is the normalized ratio of red and Near Infrared (NIR) reflectance. The NDVI ranges from −1 to +1. The value of −1 indicates very little or no vegetation activity and values closer to +1 indicate lush vegetation. A detailed description of how MOD11A1.006 and MOD13A2.006 are used in the present study is given in the Methodology (Section 3). Additionally, MOD15A2H version-6 [39] is used for deriving the combined Leaf Area Index (LAI) of the study area. MOD15A2H-006 is a global-composite dataset (The LAI algorithm picks the most suitable value for each pixel from the Terra sensor from an 8-day window) with 500 m spatial resolution. Furthermore, albedo data from band 20 of MODTBGA, MODIS [40] are used for the RZSM simulations in the present study. The MODTBGA Version 6 of the Terra MODIS collection is a daily global dataset with a 1 km spatial resolution.

2.3. C-Band Derived Soil Moisture from AMSR-2

Advanced Microwave Scanning Radiometer-2 (AMSR-2) measures the weak microwave emissions from the Earth's surface as well as the atmosphere [21]. The sensor has been providing measurements on soil moisture, precipitation, sea surface temperature, snow cover, water vapor, sea ice concentration, winds, and cloud liquid water since 2 July 2012. The soil moisture downscaling algorithm used in the present study uses the daytime and nighttime (ascending and descending) soil moisture data from AMSR-2 with a spatial resolution of 25 km. The present study utilized AMSR2/GCOM-W1 surface soil moisture (LPRM) L3 1 day 25 km × 25 km ascending V001 (LPRM_AMSR2_A_SOILM3) and AMSR2/GCOM-W1 surface soil moisture (LPRM) L3 1 day 25 km × 25 km descending V001 (LPRM_AMSR2_D_SOILM3), which are the gridded level-III data sets obtained from AMSR-2 using Land Parameter Retrieval Model (LPRM) [41]. The AMSR-2 data have been previously validated at various ground stations as part of the International Soil Moisture Network (ISMN) [42]. The same has been validated at Indian sites also, where in LPRM datasets, C-band products had R equal to 0.621 and an average unbiased RMSE of 0.07 [23]. Volumetric soil moisture from 6.9 GHZ (C Band) of daytime and nighttime is used in the present study.

2.4. Field and Ancillary Datasets

The soil texture data at the HydraProbe site were based on percentages of sand and clay. However, for regional assessment, the data have been utilized from the available FAO STATSGO. FAO STATSGO is a 30 s soil texture data remapped from the original global, 5 min soil texture data of the United Nations' Food and Agriculture Organization (FAO). State Soil Geographic (STATSGO) datasets are available from the NASA Center for Climate Simulation (NCCS) data portal along with further information [43]. The meteorological data, including maximum and minimum temperature, relative humidity (morning and evening), sunshine hours, and wind speed used in the simulations were collected in-situ and

also obtained from NASA-POWER (Prediction Of Worldwide Energy Resources) [44]. The elevation data are derived from Hydrological data and maps based on SHuttle Elevation Derivatives at multiple Scales (HydroSHEDS). The HydroSHEDS DEM is hydrologically conditioned with void-filling, filtering, stream burning, and upscaling through various techniques [33].

3. Methodology

A number of studies have been conducted by combining the two sensitive land parameters, NDVI and LST, to quantify soil moisture for the last couple of decades [4,45] and there is an established strong negative correlation between LST and NDVI [46,47] (Figure 2).
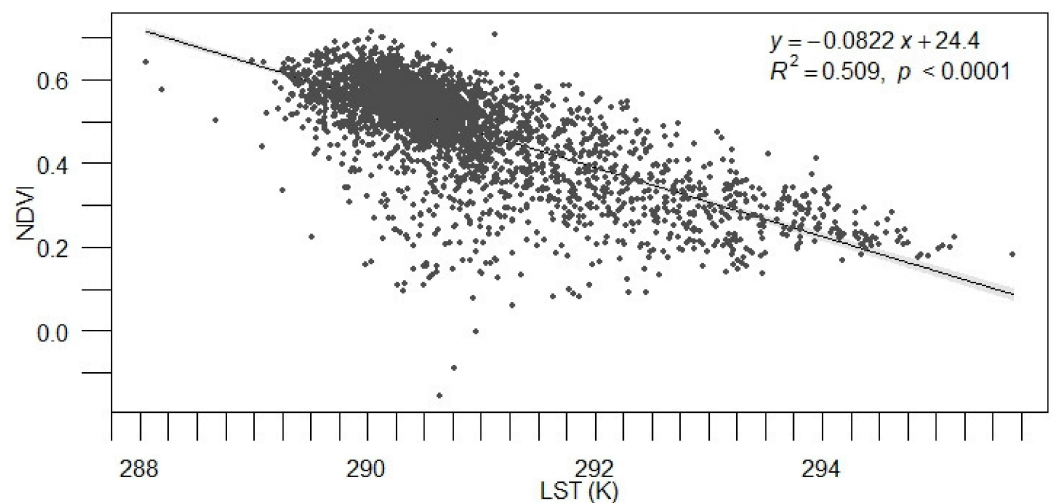
Figure 2. LST-NDVI scatter plot of the study area. LST and NDVI are chosen from corresponding LST (average of day and night) and NDVI raster of single day. The current plot shows the LST-NDVI negative correlation of 20 January 2018.

In addition, Figure 3 shows the correlation of NDVI and LST with the soil moisture in the study area. The correlation between LST-soil moisture and NDVI-soil moisture is calculated for 365 days (1 January 2018–31 December 2018). The spatial distribution of these correlation values is demonstrated in Figure 3. The correlation between NDVI and soil moisture was found to be positive. The values varied between 0.35 and 0.55 within the quantile range of 25% and 75%. In the same quantile range, the correlation between LST and soil moisture was negative (-0.43 to -0.53). The maximum correlation was 0.81 and -0.71, respectively. This method has been comprehensively tested and reviewed globally in various climatic conditions and terrain types [48]. Thus, the algorithm in the first phase of the present study downscales the 25 km C-band derived surface soil moisture from AMSR-2 to a 1 km surface soil moisture product by exploiting the strong correlations among MODIS-NDVI, MODIS-LST, and soil moisture.
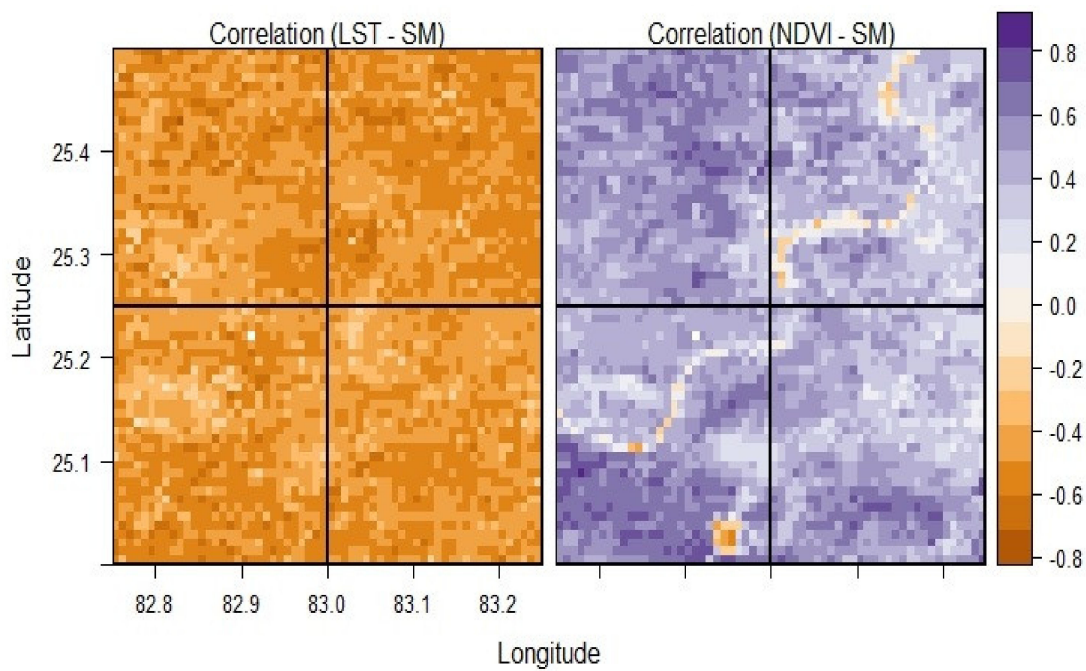
Figure 3. Correlation plot of LST and AMSR-2 soil moisture of study area (**right**). Correlation plot of NDVI and AMSR-2 soil moisture of the study area (**left**). The four AMSR-2 pixels are marked in each figure with black lines.

3.1. Downscaling AMSR-2 Surface Soil Moisture

The 16 days MODIS NDVI (MOD13A2) product is linearly interpolated to daily NDVI by considering the data acquisition date and quality. The computationally expensive processing was executed with an algorithm in R [49] by using MODIS [50] and MODISExtra [51] packages. A soil moisture downscaling algorithm based on previous work [1] is modified for the current study. The method is based on soil evaporative efficiency (SEE) in which 25 km AMSR-2 soil moisture is downscaled to 1 km. The SEE is derived from the 1 km LST and 1 km NDVI and a relationship between SEE and soil moisture is established for disaggregation. The algorithm starts by computing fractional vegetation and is calculated as below, (Equation (1)).

$$F_v = \frac{NDVI_{MODIS} - NDVI_s}{NDVI_v - NDVI_s} \tag{1}$$

where F_v is fractional vegetation cover, $NDVI_{MODIS}$ is the NDVI derived from MODIS [38], $NDVI_v$ is the NDVI fraction for the full vegetation cover, and $NDVI_s$ is the NDVI fraction for bare vegetation. Temporal computation of SEE requires skin temperature (T_s) also for each pixel. The expression used for finding the T_s is given in Equation (2).

$$T_s = \frac{LST_{MODIS} - f_v \cdot (T_{v,min} + T_{v,max})/2}{1 - f_v} \tag{2}$$

where T_s is the skin temperature and LST_{MODIS} is the pixel LST which is derived from MODIS. F_v is the fractional vegetation cover, $T_{v,max}$ and $T_{v,min}$ (min(T_{MODIS})) are the maximum and minimum temperature of the vegetated area and similarly $T_{s,max}$ (max(T_{MODIS})), and $T_{s,min}$ (min(T_{MODIS})) are the maximum and minimum temperature of bare soil. $T_{v,max}$ is estimated using the following expression, (Equation (3))

$$T_{v,max} = \min\left(\frac{LST_{MODIS} - T_{s,max}(1 - f_v)}{f_v}\right) \tag{3}$$

Soil Evaporative Efficiency (SEE) is calculated using the below expression (Equation (4)).

$$SEE = \frac{T_{s,max} - T_s}{T_{s,max} - T_{s,min}} \quad (4)$$

The relationship between SEE and soil moisture is computed for each three-month period for the present study (January 2018 to June 2018). So, the average SEE at 25 km in Equation (5) is derived for the January–March period and April to June period separately, based on Equation (4). The soil moisture at 1 km is obtained over the study area by computing the difference between the SEE at 1 km and the SEE at 25 km (Equation (5)). Additionally, the present study computed SEE and the parameters ($T_{s,max}$, $T_{s,min}$, $T_{v,max}$, and $T_{v,min}$) yearly, half-yearly, and monthly along with quarterly computations. The best results were obtained when SEE is computed quarterly because the three months period best represents the seasonal changes in the study area. The seasonality being captured in the values of LST, NDVI, and Soil moisture (AMSR-2), SEE, and downscaled soil moisture are shown in Figure 4.

$$SM_{1km} = \left(\frac{\partial SM}{\partial SEE}\right)_{25km} (SEE_{1km} - SEE_{25km}) + SM_{25km} \quad (5)$$

where SM_{1km} is the high-resolution (1 km) soil moisture calculated, SM_{25km} is the AMSR-2 soil moisture at 25 km (coarser resolution), $\partial SM/\partial SEE$ is the partial derivative of soil moisture with respect to SEE, and SEE_{1km} and SEE_{25km} are the SEE at 1 km and 25 km, respectively. The partial derivative is computed by establishing the coefficients of multiple regression between SEE and SM, as shown in Equation (6).

$$\frac{\partial SM}{\partial SEE} = a\frac{1}{N}\sum_{i=1}^{N}\frac{SM_{AMSR-2,i}}{SEE_{25km,i}} \quad (6)$$

where a is an experimental tuning parameter and N is the number of days the algorithm has been applied over the study area.

3.2. Derivation of SHPs and RZSM Simulation

Since, RZSM has a crucial role in various applications such as irrigation scheduling, flood mapping, drought estimation and even in numerical simulations of landslides, any method for retrieving RZSM at a regional scale remains significant. Thus, the estimation of subsurface soil moisture is equally important for surface soil moisture estimation. A number of studies have been undertaken to extrapolate the satellite-based surface soil moisture and quantify the root zone (up to 1 m) [52]. However, quantifying soil moisture in the root zone from the surface soil moisture is difficult because of the heterogeneity and nonlinearity of the physical processes which affect the soil moisture. On the other hand, the quantification of RZSM through a numerical model requires the input of SHPs, which in themselves are difficult to measure [22]. Thus, the second phase of the study hypothesizes that surface soil moisture downscaled from Earth observation data can be utilized to inversely derive SHPs and help in improved estimation of RZSM using HYDRUS-1D. HYDRUS-1D is a software package that comprises a one-dimensional numerical model for simulating water flow in vertical soil profiles and solute transport in variably saturated porous media [29]. HYDRUS-1D is a finite element model [29]. The model can be downloaded from the following link, https://www.pc-progress.com/en/Default.aspx?Downloads, accessed on 29 November 2022. It solves Richards' equation for soil water flow dynamics [53] based on Equation (7).

$$\frac{\partial \theta}{\partial t} = \frac{\partial}{\partial x}\left[K(h)\left(\frac{\partial h}{\partial x} + \cos\alpha\right)\right] - S \quad (7)$$

where h = water pressure head (cm), θ = water content ($cm^3 cm^{-3}$), t = time (days), x = spatial coordinate (cm) (positive upward), S = sink term ($cm^3 cm^{-3} day^{-1}$), α = angle between the

flow direction and the vertical axis and K = unsaturated hydraulic conductivity function (cm day^{-1}). A Galerkin-type linear finite element scheme is used for the spatial distribution and a Crank–Nicholson implicit finite difference scheme is used for the temporal variation of the variables in Equation (7). The simulation time step is dynamically adjusted to achieve optimal convergence of the iteration scheme. In solving Richard's equation, the water is partitioned into evapotranspiration (ET_0), runoff and RZSM. The maximum possible root water extraction rate when soil water is not limiting, i.e., the non-uniform distribution of the potential water uptake rate over a root zone was given by Equation (8):

$$S_{max} = \beta_z \times T_p \tag{8}$$

where β_z is the normalized water uptake depth, dependent on root distribution function (cm^{-1}) and T_p is the potential transpiration rate (cm day^{-1}) obtained from potential evapotranspiration, calculated by the Penman–Monteith method [54]. The Equation (9) for calculating T_p, involves using Beer's law that partitions the solar radiation component of the energy budget.

$$T_p = ET_p \left(1 - e^{-k-LAI}\right) \tag{9}$$
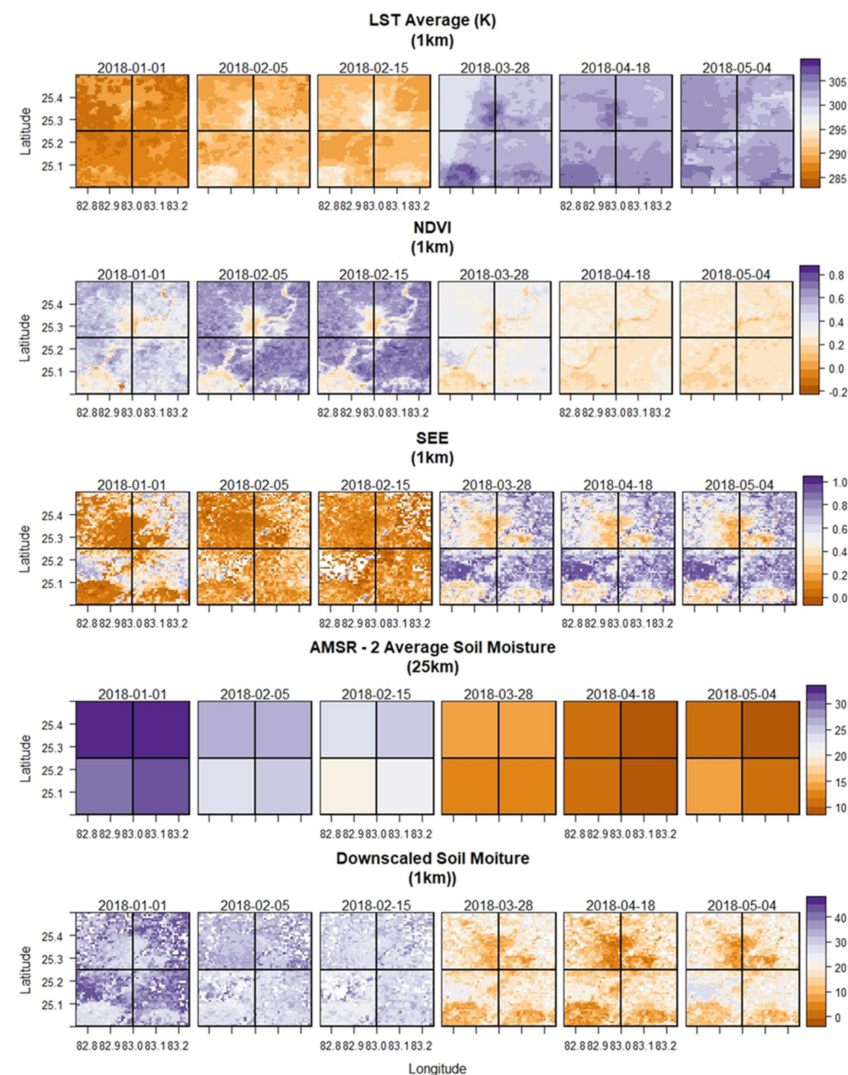
Figure 4. The seasonality captured in the values of LST, NDVI, SEE, and AMSR-2 soil moisture at 25 km resolution, and the corresponding 1 km resolution downscaled soil moisture of the selected days where the results have been compared with in-situ soil moisture.

Additionally, the albedo is utilized in the Penman–Monteith equation. The ET_0 according to the Penman–Monteith equation is as follows (Equation (10)):
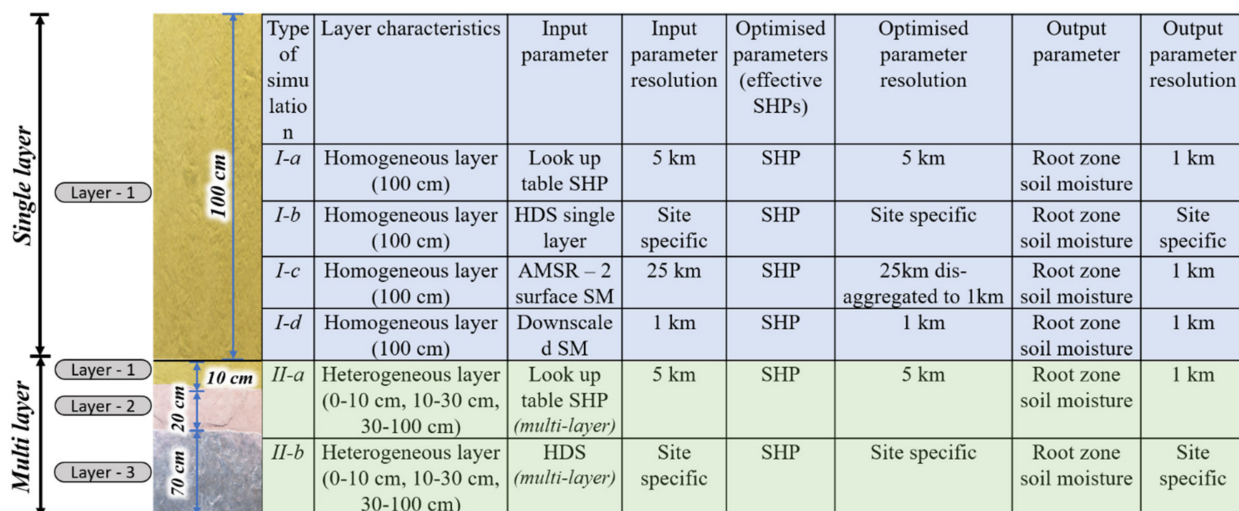
$$\lambda ET_\circ = \frac{\Delta(R_n - G) + \frac{86400\rho_a c_p(e_s^o - e_a)}{r_{av}}}{\Delta + \gamma\left(1 + \frac{r_s}{r_{av}}\right)} \tag{10}$$

where λ is the latent heat of vaporization in MJ kg^{-1}, ρ_a is air density (kg m^{-3}), C_p is the specific heat of dry air, e_s^o is mean saturated vapor pressure (kPa) computed as the mean e^o at the daily minimum and maximum air temperature (°C), r_{av} is bulk surface aerodynamic resistance for water vapor (s m^{-1}), e_a is the mean daily ambient vapor pressure (kPa), r_s is the canopy surface resistance (s m^{-1}), γ is the psychrometric constant (kPa °C^{-1}), and Rn is the net radiation. Albedo in the HYDRUS-1D is utilized to calculate the net radiation. The details of the same are available with the HYDRUS-1D [29]. For numerically solving Richard's equation, SHPs are described based on van Genuchten [55] and Mualem [22,53,56]. The required hydraulic characteristics (θ_s, θ_r, α and n) can be obtained directly from the experimental analysis of soil samples, indirectly from lookup tables, available pedotransfer functions, or determined by a best curve fitting method using in-situ soil moisture data. It has been shown previously that experimental datasets obtained through pressure plate analysis are time-consuming while lookup tables do not represent the regional areas [53]. Additionally, the pedotransfer functions require field soil analysis as most of them are based on percentages of sand, silt and clay. Moreover, pedotransfer functions developed for a region need to be used with caution at another field site as the soil conditions may be different. The current study, therefore, looks to indirectly estimate SHPs being independent of any field data. The study proposes to utilize the downscaled AMSR-2 soil moisture to inversely estimate the SHPs. Tens of thousands of iterations are carried out by using multiple sets of SHPs to generate a sequence of soil moisture (forward modeling). A range of feasible values for SHPs (saturated hydraulic conductivity (K_s), saturated soil moisture content (θ_s), residual soil moisture content (θ_r), and alpha (α) and n of the Van Genuchten equation) are generated as the uniform distribution between the upper and lower limit of SHPs. Table 1 shows the constraining boundaries of the SHPs chosen for the forward modeling. The optimized SHPs are chosen based on the minimum normalized Root-Mean-Square Error (nRMSE) with the in-situ soil moisture data. However, as already stated the in-situ soil moisture has limited availability and numerical experiments were designed to understand the impact of the usage of downscaled soil moisture as an observed dataset in deriving the SHPs at a regional scale. The details of governing numerical experiments to determine the SHPs are described below and given in Figure 5. The four treatments (*I-a, I-b, I-c, I-d*) consider the vertical soil profile homogeneous while two treatments (*II-a* and *II-b*) consider the vertical soil profile heterogenous, which represents the field conditions ideally. *I-a* numerical run is the simplest of the six numerical experiments, which considers a 100 cm deep soil profile with silt loam as only the soil type and the SHPs based on the default lookup table values in HYDRUS-1D. The lookup table values are literature values for each soil type based on the FAO (Food and Agriculture Organization) dataset. For *I-b*, HydraProbe Data record System (HDS) surface soil moisture (Figure 1) is used for inversely optimizing the SHPs with parameters in the range given in Table 1. The optimization is based on the least nRMSE between modeled surface soil moisture and HDS surface soil moisture. *I-c* is an inverse optimization simulation that takes AMSR-2 satellite-derived, daily, 25 km soil moisture data as input and estimates the SHPs. The parameters are optimized based on the minimization of nRMSE between the modeled surface soil moisture data and the AMSR-2 soil moisture. *I-d* is again an inverse optimization where downscaled surface soil moisture product from the first phase of the study has been utilized to obtain the effective SHPs. Method *I-d* has the advantage of being independent of the in-situ soil moisture data, required in experiment *I-b* and has a finer spatial resolution as compared to experiment, *I-c*. So, it is hypothesized in this study that method, *I-d*, can result in providing high-resolution RZSM for agricultural zones

where in-situ soil moisture datasets are limited or even missing and further help with designing water management policies. The robustness of the method is further tested with two more experiments, which consider heterogeneous soil layers (*II-a* and *II-b*). *II-a* is based on heterogeneous layers (0–15 cm, 15–30 cm and 30–100 cm) in the soil profile (Figure 5). The SHPs for the three layers are based on the default lookup table values. The lookup table values are literature values for each soil type based on the built-in Rosetta module in HYDRUS-1D. The soil type for the study area is based on in-situ data collection. The final treatment, *II-b* takes into consideration the in-situ soil moisture for all three layers to inversely optimize the SHPs for the three layers. The summary of these experiments is given in Figure 5 and the flowchart of the optimization methodology is shown in Figure 6. Finally, the derived SHPs are utilized with model boundary conditions to simulate RZSM.

Table 1. Upper and lower limit of SHPs (range of SHPs) used in the study area. The upper and lower limits of the SHPs have been chosen to include a set of possible values of SHPs so that the simulation in HYDRUS-1D will be realistic and non-repetitive.

SHPs	Ks	θ_s	θ_r	α	n
Lower Limit	15	0.35	0.01	0.0007	1
Upper Limit	35	0.43	0.07	0.1	2

Type of simulation	Layer characteristics	Input parameter	Input parameter resolution	Optimised parameters (effective SHPs)	Optimised parameter resolution	Output parameter	Output parameter resolution
I-a	Homogeneous layer (100 cm)	Look up table SHP	5 km	SHP	5 km	Root zone soil moisture	1 km
I-b	Homogeneous layer (100 cm)	HDS single layer	Site specific	SHP	Site specific	Root zone soil moisture	Site specific
I-c	Homogeneous layer (100 cm)	AMSR − 2 surface SM	25 km	SHP	25km dis-aggregated to 1km	Root zone soil moisture	1 km
I-d	Homogeneous layer (100 cm)	Downscaled SM	1 km	SHP	1 km	Root zone soil moisture	1 km
II-a	Heterogeneous layer (0-10 cm, 10-30 cm, 30-100 cm)	Look up table SHP (multi-layer)	5 km	SHP	5 km	Root zone soil moisture	1 km
II-b	Heterogeneous layer (0-10 cm, 10-30 cm, 30-100 cm)	HDS (multi-layer)	Site specific	SHP	Site specific	Root zone soil moisture	Site specific

Figure 5. Details of the experiments with the input data sets, based on which the SHPs are optimized.

Model Initial and Boundary Conditions

Atmospheric boundary condition or the flux type upper boundary condition was applied for one-dimensional soil moisture movement with Equation (11) being the initial condition and Equation (12) being the upper boundary condition. The bottom boundary condition considered in the current study is free drainage (Equation (13))
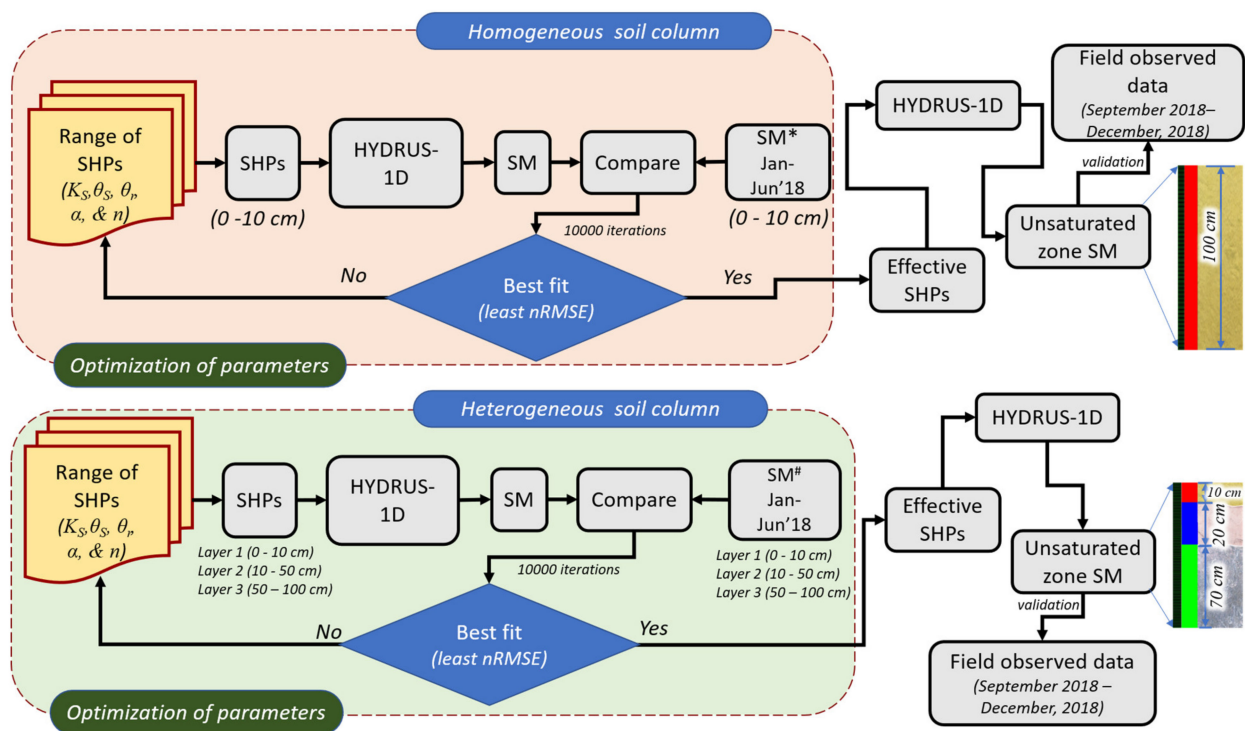
$$\theta(z,t) = \theta_i(z,0), for - L \le z \le 0 \tag{11}$$

where θ_i is the initial soil moisture content and L = depth of soil profile.

$$- K(h)\left(\frac{\partial h}{\partial z} + 1\right)\bigg|_{z=0} = q_0(t) \text{ for } t > 0 \tag{12}$$

where q is the soil moisture flux, and q_0 is the initial value of soil moisture flux on the surface.

$$\frac{\partial h}{\partial z} = 0, \; z = -L \tag{13}$$

Figure 6. The methodology adopted for optimization of SHPs for the homogeneous and heterogeneous soil column for calibration and validation period. SM indicates the soil moisture from HYDRUS-1D. SM* indicates the soil moisture datasets such as HDS in-situ data (*I-b* treatment), AMSR-2 at 25 km² (*I-c* treatment), and Downscaled soil moisture at 1 km² (*I-d* treatment) with which optimization is achieved in homogeneous soil column. SM# indicates the soil moisture dataset from HDS in-situ soil moisture (*II-b*).

3.3. Statistical Analysis for Model Performance

The major parameters considered for analysis of results and model outputs in the current study are (ANalysis Of Variance) ANOVA, nRMSE, and Correlation. ANOVA is a statistical technique that compares sample populations based on their means and spread of the data (variance). The ANOVA coefficient, F, is calculated by the ratio between MST (mean sum of the squares due to treatment) and MSE (mean sum of errors due to error). Correlation is a statistical tool to quantify the linear relationship between two variables without considering the cause and effect and the correlation coefficient; r measures the extent of the relationship.

$$r = \frac{\Sigma(x_i - \overline{x})(y_i - \overline{y})}{\sqrt{\Sigma(x_i - \overline{x})^2 \Sigma(y_i - \overline{y})^2}} \tag{14}$$

where r = correlation coefficient, x_i = values of the x variable in the sample, $\overline{x}$ = mean of the values of the x variable, y_i = values of the y variable in the sample, and $\overline{y}$ = mean of the values of the y variable.

Root Mean Square Error/Deviation (RMSE or RMSD) denotes the difference between the simulated values from the model or algorithm and ground-measured values. The present study uses Normalized Root Mean Square Error (nRMSE) and is calculated as,

$$nRMSE = \frac{RMSE}{\overline{y}} \tag{15}$$

where $\bar{y}$ = mean of the observed data sets; RMSE is computed between the output soil moisture and in-situ soil moisture,

$$RMSE = \sqrt{\frac{\sum_{i=1}^{N}(x_i - \hat{x}_1)^2}{N}} \tag{16}$$

where N = number of non-missing data points, i = variable i, x_i = actual observation time series, and $\hat{x}_1$ = simulated values or model output time series. The selection of best-fit simulation in the study is achieved through normalized RMSE which enables the comparison of datasets with different scales. A schematic diagram of major input and output parameters and cardinal steps in the methodology is shown in Figure 7. The study has been carried out in two interlinked stages and the output from the first stage of the study is used in the second stage for the derivation of SHPs and RZSM.
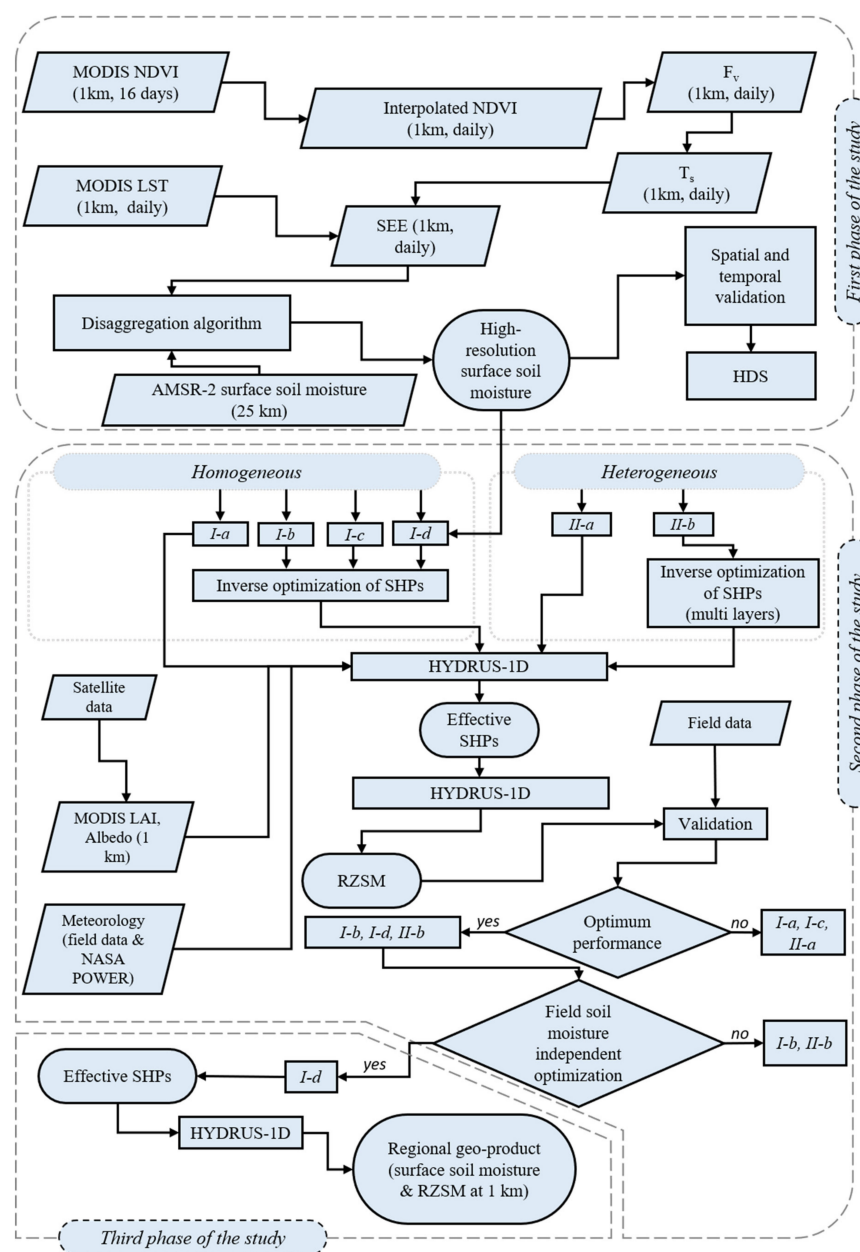

Figure 7. Outline of the methodology of the present study. *I-a, I-b, I-c, I-d, II-a,* and *II-b* are explained in Section 3.2. Refer to Figure 5 for details about the treatments and resolution of the input and output datasets.

4. Results

In the present study, the downscaled AMSR-2 soil moisture from the algorithm is compared with the ground measurements in two comprehensive ways viz. a continuous daily comparison with the HydraProbe (temporal) dataset and with surface ground measurements at 44 locations (spatial).

4.1. Temporal Validation of Downscaled Soil Moisture

Figure 8 shows the plot of in-situ soil moisture at the validation site with the corresponding soil moisture from the downscaled product and also with the AMSR-2 soil moisture. The downscaled soil moisture has a correlation of 0.73 at the validation site (1 January 2018 to 11 June 2018) whereas AMSR-2 soil moisture has a much lesser (0.58) correlation during the same period with the in-situ soil moisture data. Additionally, the correlation between original AMSR-2 and downscaled AMSR-2 soil moisture is 0.62. Although the downscaled AMSR-2 soil moisture is not able to capture the sudden spikes observed in the in-situ soil moisture data, it fairly follows the trend. The spikes may have been the result of the irrigation rather than any kind of precipitation. In the year 2018, 6 months of downscaled soil moisture values have been validated with the in-situ soil moisture and an nRMSE of 0.44 is calculated for the validation site.
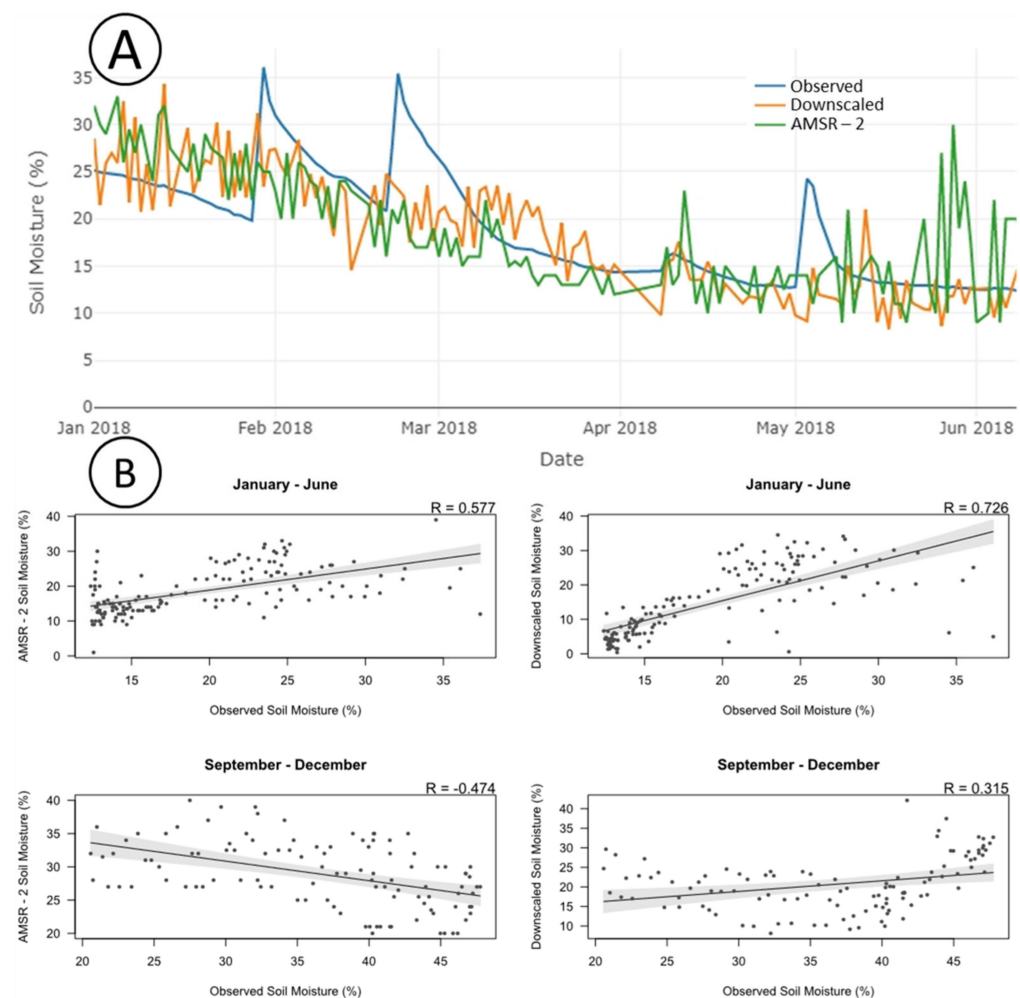
Figure 8. (**A**) Comparison of ground-measured soil moisture at the study site versus the corresponding soil moisture from the downscaled product with the AMSR-2 soil moisture from 1 January 2018 to 11 June 2018 (line-plot). (**B**) Scatterplot of in-situ soil moisture and AMSR-2 soil moisture and scatterplot of in-situ soil moisture and AMSR-2 downscaled soil moisture.

From 1 September 2018 to 31 December 2018 the downscaled soil moisture has a 32% correlation with the in-situ data. The correlation between in-situ soil moisture data and downscaled soil moisture data for September–December period is low because the input satellite data (AMSR-2) used in the algorithm have a negative correlation with the in-situ soil moisture data. Since the algorithm used in the present study depends on the quality of the input data sets, the downscaled product has a poor positive correlation with in-situ soil moisture. It is worth mentioning that the algorithm could derive high-resolution soil moisture with better correlation from a satellite dataset which was actually having a negative correlation with the in-situ data. Figure 8 shows four scatter plots that depict the behavior of downscaled soil moisture data and AMSR-2 data in the study area during the January–June and September–December periods.
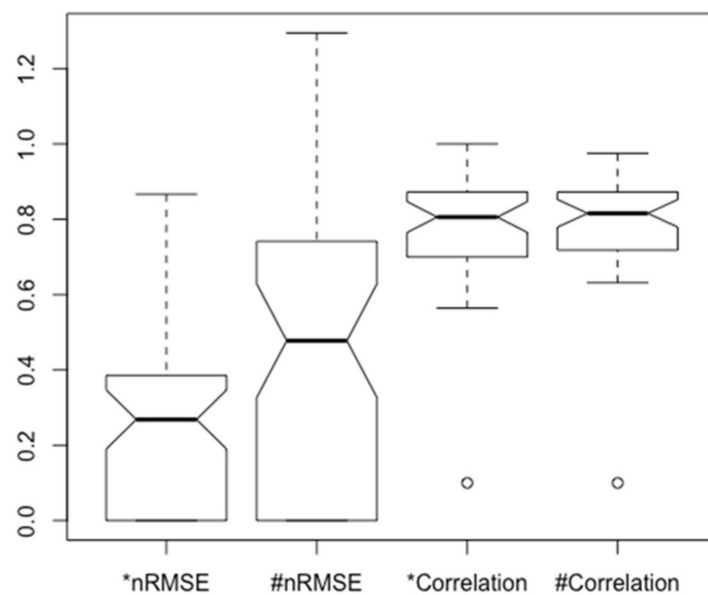
4.2. Spatial Validation of Downscaled Soil Moisture

The two parameters, LST and NDVI have been utilized in the downscaling of AMSR-2 soil moisture and the descriptive statistics of these parameters on six dates, when the surface soil moisture was collected are shown in Table 2. The range shown is the data that lie between the first and third quartiles.

Table 2. Descriptive statistics of LST, NDVI, SEE, AMSR-2, and Downscaled soil moisture for the selected six days. * The values in brackets represent the median value of the spatial data.

Variables	1 January 2018	5 February 2018	16 February 2018	28 March 2018	18 April 2018	4 May 2018
LST	286–288 * (287.11)	289.82–291.62 (290.60)	289.98–291.66 (291.07)	300.71–302.65 (301.53)	302.45–303.47 (302.80)	301.84–303.64 (302.86)
NDVI	0.48–0.66 (0.44)	0.28–0.35 (0.60)	0.48–0.66 (0.61)	0.28–0.35 (0.32)	0.22–0.26 (0.24)	0.20–0.24 (0.22)
SEE	0.07–0.49 (0.28)	0.09–0.25 (0.16)	0.07–0.19 (0.12)	0.44–0.75 (0.60)	0.46–0.76 (0.61)	0.45–0.75 (0.60)
AMSR-2 SM	30.75–32.00 (31.50)	24.75–26.25 (25.50)	21.75–23.75 (22.75)	13.00–13.50 (13.25)	10.00–11.00 (10.50)	10.75–11.75 (11.00)
Downscaled SM	28.97–39.16 (34.25)	27.51–32.78 (30.34)	25.99–29.85 (27.68)	12.35–20.06 (16.43)	9.35–17.29 (13.68)	13.00–21.00 (17.58)

It can be seen in Figure 4 that with the utilization of the downscaling algorithm, spatial heterogeneity of the data is achieved for the six dates. Figure 9 depicts the boxplot of nRMSE and the correlation of downscaled soil moisture and original AMSR-2-derived soil moisture with the in-situ soil moisture at 44 validation sites. The comparison of downscaled soil moisture shows a very good correlation with the field measurements. It shows an above 70% correlation at nearly 38 stations and five stations show a correlation between 50% and 70%; 36 validation sites have nRMSE less than 1 between in-situ data and downscaled soil moisture with the highest nRMSE being 1.599 and the lowest being 0.141. The median of the nRMSE of downscaled soil moisture is just above 0.2 and the corresponding AMSR-2 soil moisture has a median above 0.4. The outliers in the plot represent six validation sites where the correlation is fairly low. It is evidently clear from the comparison of the boxplots (Figure 9) that the downscaled soil moisture is significantly closer to the in-situ soil moisture data with a substantially better spatial resolution.

Figure 9. Boxplot of nRMSE and correlation of downscaled soil moisture and original AMSR-2 derived soil moisture, with the in-situ surface soil moisture at 44 validation sites. * Is for metrics between downscaled soil moisture and in-situ surface soil moisture. # Is for metrics between AMSR-2 soil moisture and in-situ surface soil moisture.

4.3. Impact on Surface Soil Moisture and RZSM Simulation Based on Estimated SHPs

The RZSM simulations corresponding to the homogeneous and heterogeneous soil profiles are validated at the HydraProbe site while the surface soil moisture simulations are validated both at the HydraProbe site and 44 sites.

4.3.1. Impact of Homogeneous Soil Profile

The indirectly estimated SHPs of best-fit iteration based on the least nRMSE from the 10,000 iterations for all the methods are given in Table 3. Figure 10 shows the dotty plots representing the 10,000 iterations, for the SHPs based on the two numerical experiments (*I-b* and *I-d*). The blue dots represent the single parameter combination from 10,000 iterations with the least nRMSE. Table 3 has the correlation and nRMSE between the modeled and in-situ soil moisture data for the calibration (January 2018–June 2018) period during which the SHPs are derived for all the numerical experiments. The derived SHPs are further utilized in the model to obtain the soil moisture for the three soil layers (surface, 20 cm, and 50 cm) during the validation period (September 2018–December 2018), with correlation and nRMSE being mentioned in Table 3. The soil moisture output from the *I-b* and *I-d* treatments has a very good correlation with the HDS data at the considered depths as seen in Table 3 and Figure 11. *I-a* and *I-c*-derived SHPs have reduced performance among the four treatments, which illustrates the significance of site-specific derivation of SHPs for better soil moisture modeling (Figure 11).

Table 3. Summary of the experiments, nature of the corresponding soil profile and soil depth, optimized SHPs, and correlation and nRMSE of output soil moisture from each experiment in calibration and validation period.

Soil Profile	Experiment No.	Soil Depth (cm)	Soil Hydraulic Parameters					Soil Depth (cm)	Calibration		Validation	
			Ks	*θs*	*θr*	*α*	*n*		*Cor*	*nRMSE*	*Cor*	*nRMSE*
Homogeneous	*I-a*	0–100	10.80	0.45	0.07	0.0200	1.41	0–15	0.49	0.38	0.78	0.50
								15–30	0.32	0.43	0.92	0.22
								30–100	0.09	0.16	0.98	0.18
	I-b	0–100	31.66	0.43	0.03	0.0008	1.31	0–15	**0.76**	**0.25**	**0.96**	**0.34**
								15–30	0.70	0.19	0.91	0.28
								30–100	0.81	0.24	0.98	0.31
	I-c	0–100	20.67	0.35	0.07	0.0011	1.24	0–15	0.73	0.27	0.91	0.43
								15–30	0.67	0.25	0.9	0.35
								30–100	0.78	0.18	0.98	0.37
	I-d	0–100	32.54	0.42	0.04	0.0009	1.33	0–15	**0.76**	**0.25**	**0.96**	**0.37**
								15–30	0.71	0.18	0.91	0.31
								30–100	0.82	0.25	0.98	0.34
Heterogeneous	*II-a*	0–15	10.80	0.45	0.07	0.0200	1.41	0–15	0.45	0.39	0.81	0.48
		15–30	10.80	0.45	0.07	0.0200	1.41	15–30	0.19	0.37	0.92	0.22
		30–100	1.68	0.43	0.09	0.0100	1.23	30–100	−0.35	0.29	0.98	0.1
	II-b	0–15	16.57	0.36	0.01	0.0500	1.163	0–15	**0.73**	**0.27**	**0.87**	**0.43**
		15–30	22.81	0.39	0.07	0.0600	1.05	15–30	0.68	0.39	0.91	0.55
		30–100	24.86	0.43	0.02	0.0240	1.324	30–100	0.53	0.42	0.98	0.48
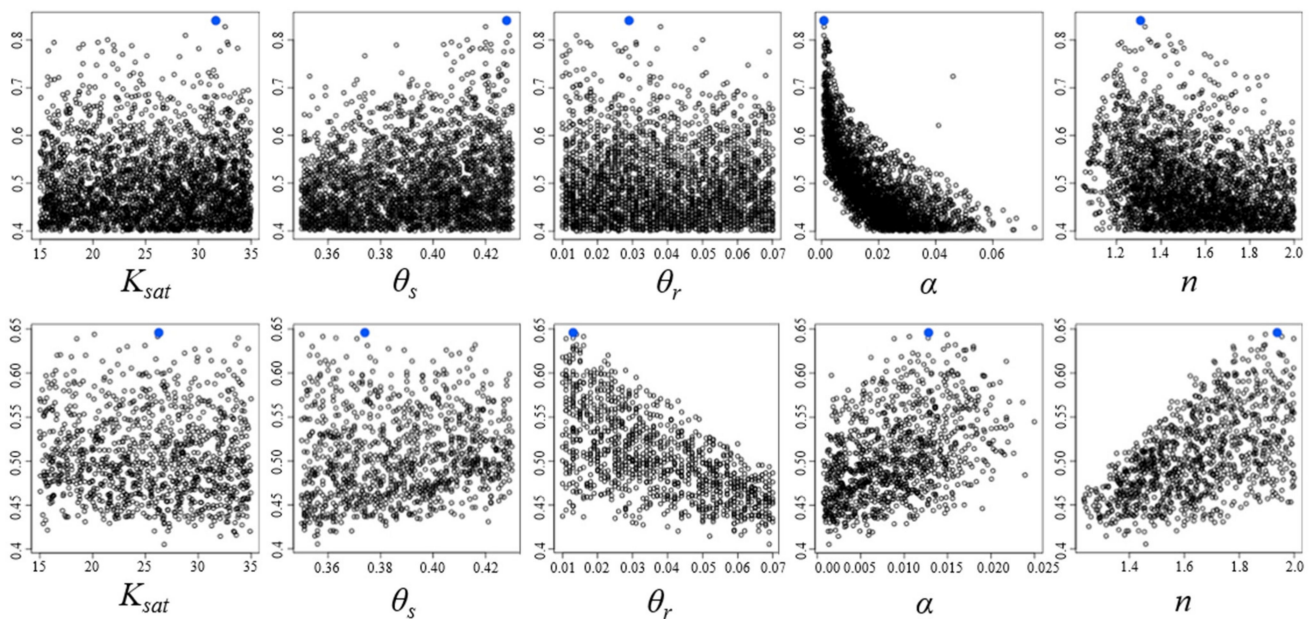
Figure 10. Dotty plots, for the parameters considered for the two runs (*I-b* and *I-d*). The blue dots represent the parameter combination (optimized parameter) with nRMSE. The y-axis shown here represents the correlation. K_{sat}, θ_s, and θ_r are saturated hydraulic conductivity, saturated water content, and residual water content, respectively. α is related to the inverse of the air entry suction and n is a measure of the pore-size distribution.
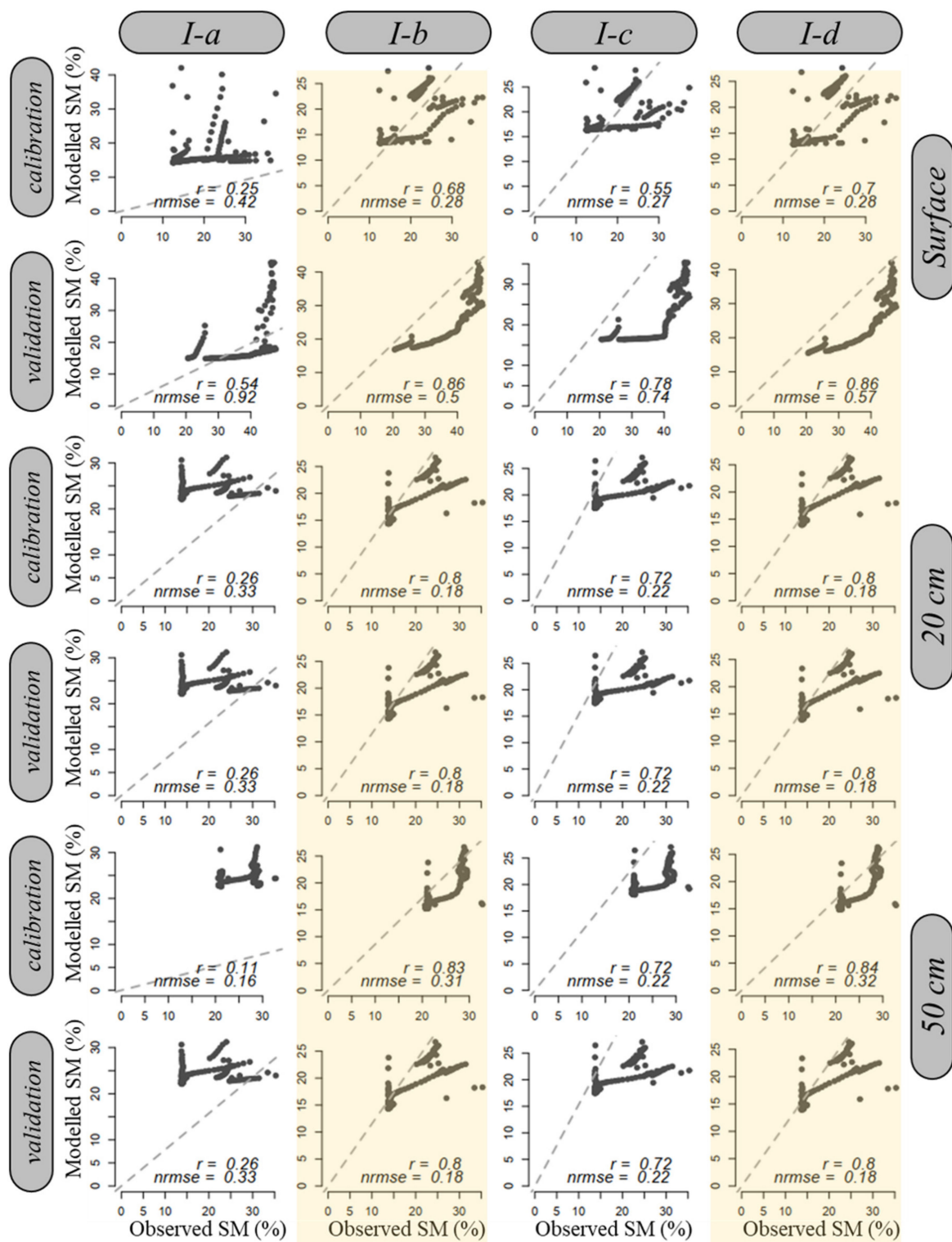
Figure 11. Comparison of the output soil moisture from *I-a*, *I-b*, *I-c*, and *I-d* treatments corresponding surface, 20 cm, and 50 cm deep layers with HDS soil moisture. Plots corresponding to each layer's (surface, 20 cm, and 50 cm) calibration and validation are plotted.

The *I-a* simulation showed a low correlation below 25% (Table 3) with the HDS dataset's 0 cm (surface), 20 cm deep (second), and 50 cm (third) deep soil moisture. The corresponding nRMSE of the modeled soil moisture for the respective surface, first, and second layers are 0.37, 0.43, and 0.16. This run is usually a default run that is carried out

in the absence of *in-situ* SHPs. The *I-b* simulation has a high correlation for the surface and 20 cm soil depth for both calibration and validation period. However, it can be seen that the model is not able to have a correlation for the 50 cm soil depth with the chosen SHPs. The *I-c* treatment uses AMSR-2 soil moisture data (25 km) to obtain SHPs followed by simulating the RZSM. This treatment has a poor correlation being below 25% for all three soil depths with the HDS data. The *I-d* simulations, which consider the homogeneous soil profile, use the high-resolution downscaled AMSR-2 soil moisture data derived in the first phase of this study. The model shows an improvement in correlation as compared to *I-a* and *I-c* for the surface soil moisture simulation and is comparable to *I-b* being at 70%. This simulation is seen to be a better scenario as the correlation in the calibration period is maintained high for all three layers of the soil profile. Even for the validation period, the *I-d* treatment can be seen to outperform the *I-a* and *I-c* with better performance at 50 cm also as compared to *I-b*. These experiments suggest that the *I-d* method can be a robust method, wherein the SHPs are estimated independent of in-situ data and RZSM is obtained at high spatial (1 km) and temporal resolution (1 day). Secondly, this method can be used in the ungauged areas as the input data are mostly Earth observation-based datasets and can help with the determination of agricultural water demands based on soil moisture. Figure 11 compares the output soil moisture from *I-a, I-b, I-c,* and *I-d* treatments corresponding to the surface, 20 cm deep, and 50 cm deep layers.

4.3.2. Impact of Heterogeneous Soil Profile

The other two runs considered in the study, *II-a* and *II-b* were conducted by introducing the heterogeneity in the soil profile. These two runs, however, are not independent of in-situ data. *II-a* required the soil type information for the three layers and then was run on the default lookup tables. Even considering the heterogeneous soil layer, the default SHPs (Table 3) were not able to correlate as highly as the *I-c* treatment for the calibration period. The validation period showed some high correlation (0.59–0.92), which means the default SHPs are suited for the winter period of the region. However, in the absence of in-situ data, it will be difficult to ascertain the validity of this method if utilized for agricultural water management policies. On the other hand, the *II-b* run, based on in-situ soil moisture for all three depths had a high correlation for both the calibration and validation period being in the range of 0.40–0.82 and 0.94–0.95, respectively. This method is best as compared to all the six treatments considered in the present study. However, this method is totally dependent on the HDS, which is not the scenario in most agricultural field locations. The availability of a continuous in-situ soil moisture dataset is lacking. So, this treatment even if it provides the best set of SHPs at the site, its usage at any other location becomes negligible. Thus, it can be seen again that *I-d* treatment, which considers downscaled soil moisture from AMSR-2 data can be relied upon with some improvement required for the wet season.

4.3.3. Rootzone Soil Moisture Geo-Product at High Temporal and Spatial Scale

The *I-d* method, which is shown to have performed well at the HDS site, was used to spatially simulate the soil moisture using HYDRUS-1D for the 44 sites. Table 4 shows the optimized SHPs for each of the 44 HDS sites corresponding to the best iteration (minimum error). These SHPs are fed to HYDRUS-1D for the simulation of soil moisture at 44 locations. Even though these locations are geographically not very close to each other (Figure 1), these 44 sites fall under a single soil type, loam (FAO Soil texture), which would contribute the same set of SHPs for all the sites. The present study could estimate the SHPs for each location rather than choosing a single value for a fairly large geographic extent through inverse simulation of SHPs in HYDRUS-1D with high-resolution downscaled soil moisture as input. At these 44 sites, the modeled surface soil moisture was compared with the in-situ surface soil moisture. Figure 12a shows the in-situ and modeled surface soil moisture (*I-a* and *I-d*) over the study site as a spatial dataset with a time series of selected stations as shown in Figure 12b. Figure 12b also has time series with SHPs based on FAO soil type (treatment *I-a*). The time series is plotted with Nash-Sutcliffe Efficiency (NSE). It can be

seen from the plot that the SHPs impact the soil moisture simulations. The *I-a* experiment has the same soil moisture simulation for each location as compared to the *I-d* treatment. Further, the SHPs at Location 6 have let the NSE to be improved from 30% to 80%. It can also be seen from Figure 12c, that the mean NSE improved from 0.10 to 0.50. Additionally, the mean nRMSE was found to reduce from 0.50 to 0.31. The range of nRMSE decreased from 0.24–0.66 to 0.20–0.32. The ANOVA test was significant at $p = 0.10$, showing that the change in SHPs values resulted in a change in soil moisture simulations. The mean correlation for all the stations was found to be 60%. The quantile range (0.25, 0.75) for the correlation was 39%–68% with the maximum correlation being 88%. This analysis shows that the treatment, *I-d* can be utilized in the absence of a real in-situ soil moisture dataset and we can simulate high-resolution soil moisture both spatially and temporally. Figure 13 shows the rootzone soil moisture product based on *I-a* and *I-d* treatment. It can be seen that there is no spatial variation at a time for *I-a* simulation as SHPs remain the same. On the other hand, there is variation in the rootzone soil moisture in the case of *I-d* treatment. The rootzone soil moisture is important to understand the deficit as it plays an important role in determining the irrigation depth. The geo-product can be helpful for the water management policies in the region as the soil moisture product can be utilized for further processing of the soil moisture deficit [57,58], the quantification of irrigation water demand and it can be replicated in other areas as well. Even though the results look promising, the study is limited, and more validation is required.

Table 4. SHPs of 44 HDS sites corresponding to the best iteration (minimum error).

Station	Ks	θs	θr	α	n	Station	Ks	θs	θr	α	n
HDS-01	18.47	0.41	0.01	0.047	1.15	HDS-23	34.97	0.38	0.07	0.022	1.14
HDS-02	21.95	0.37	0.04	0.046	1.35	HDS-24	29.78	0.40	0.05	0.018	1.29
HDS-03	21.98	0.42	0.05	0.005	1.60	HDS-25	22.05	0.37	0.06	0.042	1.78
HDS-04	17.11	0.42	0.06	0.024	1.04	HDS-26	24.62	0.37	0.07	0.052	1.08
HDS-05	17.11	0.42	0.06	0.024	1.04	HDS-27	23.75	0.40	0.03	0.062	1.65
HDS-06	24.65	0.39	0.06	0.017	1.59	HDS-28	17.53	0.38	0.02	0.042	1.80
HDS-07	24.54	0.43	0.05	0.085	1.86	HDS-29	15.55	0.42	0.06	0.039	1.83
HDS-08	17.11	0.42	0.06	0.024	1.04	HDS-30	29.78	0.40	0.05	0.018	1.29
HDS-09	23.65	0.39	0.07	0.002	1.73	HDS-31	23.23	0.38	0.05	0.002	1.10
HDS-10	21.98	0.42	0.05	0.005	1.60	HDS-32	33.71	0.40	0.05	0.008	1.14
HDS-11	22.05	0.37	0.06	0.042	1.78	HDS-33	32.18	0.39	0.01	0.006	1.14
HDS-12	17.53	0.38	0.02	0.042	1.80	HDS-34	23.73	0.41	0.05	0.005	1.18
HDS-13	29.78	0.40	0.05	0.018	1.29	HDS-35	22.68	0.38	0.02	0.008	1.08
HDS-14	21.95	0.37	0.04	0.008	1.04	HDS-36	22.34	0.39	0.07	0.008	1.11
HDS-15	34.43	0.41	0.04	0.085	1.00	HDS-37	28.52	0.42	0.03	0.010	1.07
HDS-16	23.75	0.40	0.03	0.062	1.65	HDS-38	22.68	0.38	0.02	0.008	1.08
HDS-17	24.11	0.36	0.02	0.023	1.04	HDS-39	21.5	0.43	0.05	0.015	1.06
HDS-18	20.57	0.42	0.04	0.079	1.84	HDS-40	27.65	0.37	0.02	0.095	1.46
HDS-19	24.52	0.42	0.05	0.064	1.74	HDS-41	22.26	0.39	0.07	0.049	1.38
HDS-20	34.29	0.37	0.04	0.057	1.46	HDS-42	18.1	0.36	0.01	0.012	1.10
HDS-21	24.11	0.36	0.02	0.023	1.04	HDS-43	21.09	0.39	0.04	0.006	1.12
HDS-22	34.29	0.37	0.04	0.057	1.46	HDS-44	18.39	0.36	0.04	0.007	1.10

(**a**)

(**b**)

Figure 12. *Cont.*

(**c**)
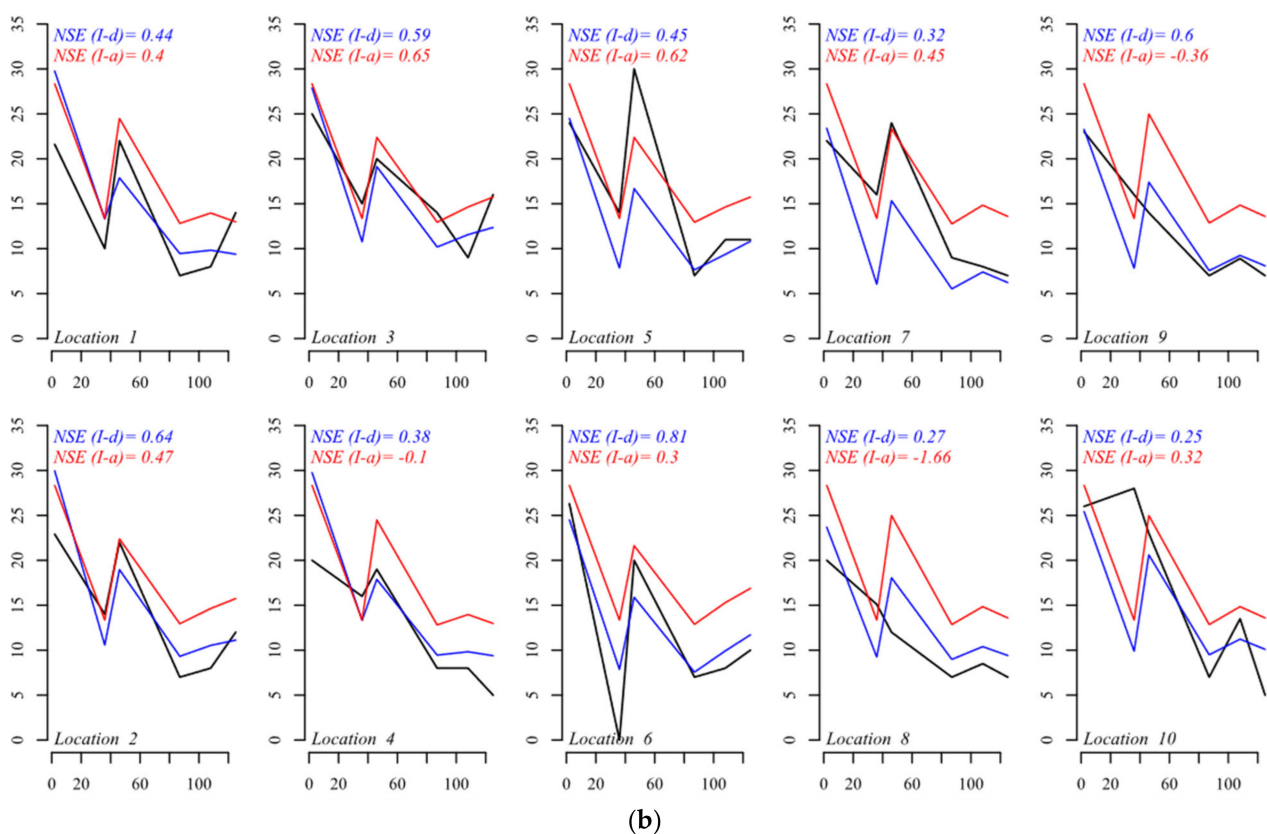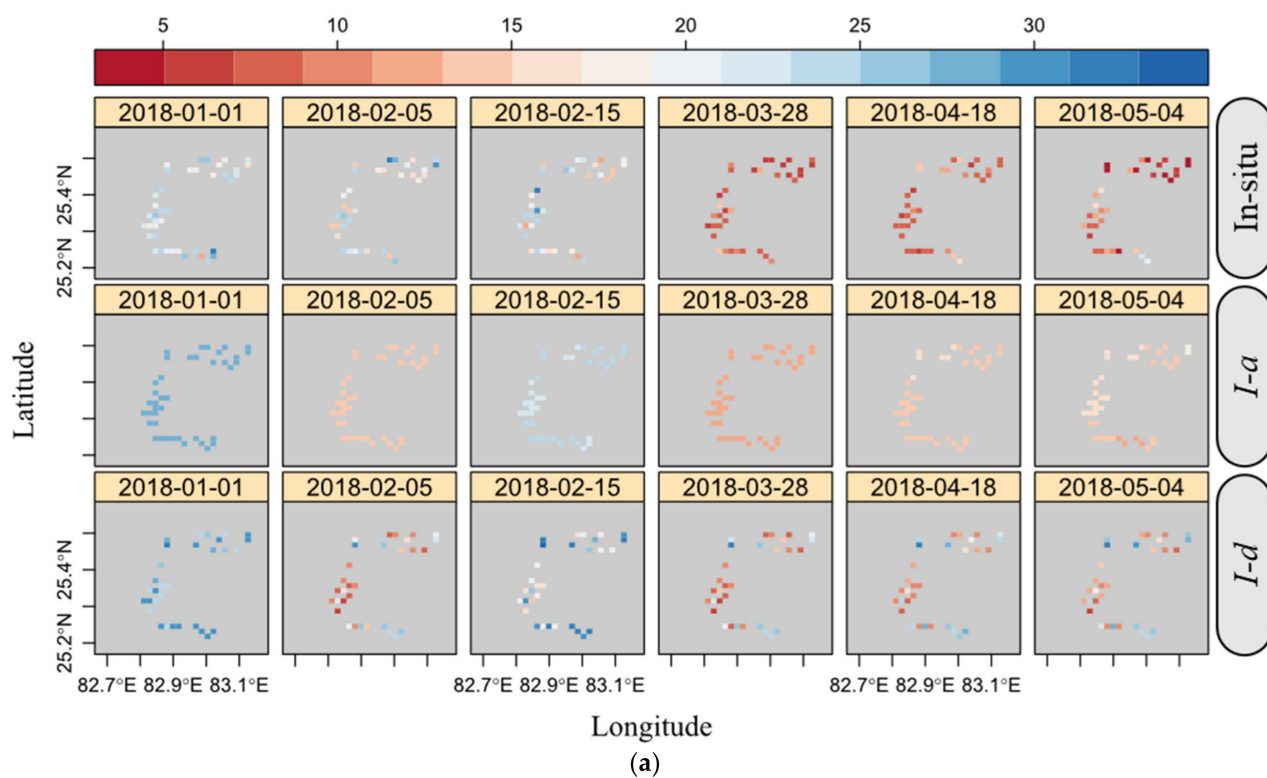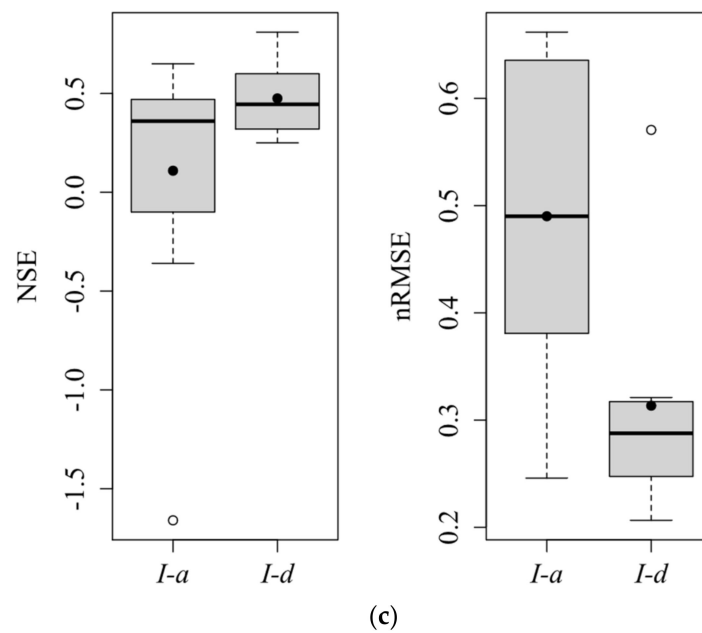
Figure 12. (**a**) Spatial derivation of surface soil moisture at 44 locations. The in-situ soil moisture and modeled soil moisture from *I-a* and *I-d* treatments are plotted for six days during the study period. (**b**) Time series of soil moisture simulations at 10 locations. The x-axis denotes the simulation days (Julian days) and y-axis denotes the soil moisture (%). Blue line represents the soil moisture simulations based on *I-d* experiment while red line denotes the soil moisture simulations based on *I-a* experiment. Black line represents the in-situ soil moisture. (**c**) Boxplot representation of NSE and nRMSE for the surface soil moisture at the 44 locations. The black dot represents the mean of the data.
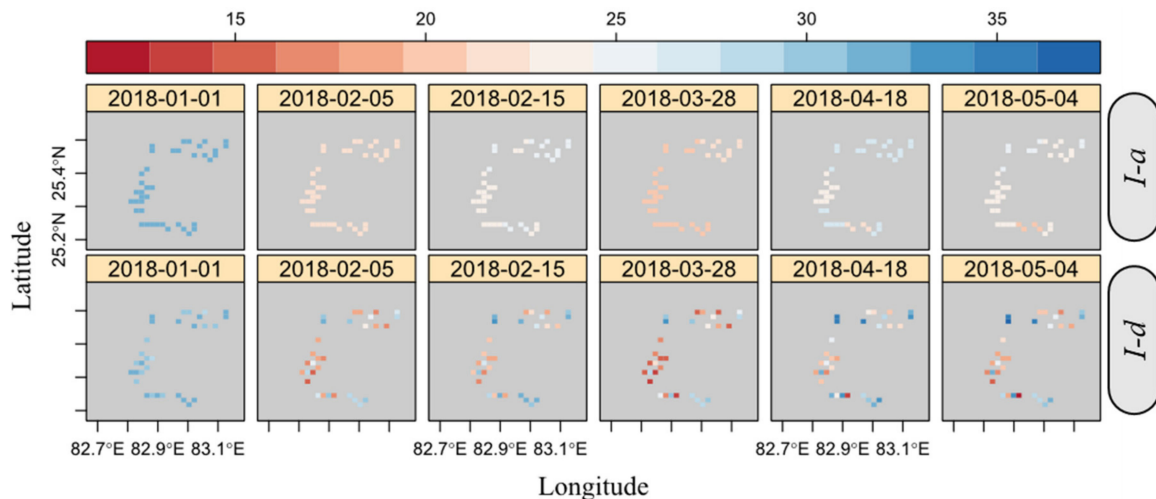
Figure 13. Modelled RZSM simulations for six days during the study period. The simulated *I-a* and *I-d* RZSM for 44 locations in the study area are plotted.

5. Discussion

The current study has focused on estimating the high-resolution SHPs using the downscaled AMSR-2 soil moisture. A downscaling algorithm utilized two optical datasets, NDVI and LST. However, the study has some limitations, such as the linear interpolation of non-linear data, NDVI could lead to errors in the AMSR-2 soil moisture downscaling. NDVI is dependent on the phenological stages of the cropped areas and interpolation can lead to some erroneous values, especially during the transitional period from a cropped period to a bare zone. Additionally, the aggregation of NDVI and LST to a 25 km resolution for developing the relationship with the AMSR-2 soil moisture dataset may lead to errors.

However, even with the above-stated uncertainties, the algorithm is well-established and has been widely accepted. The high-resolution downscaled surface soil moisture has been further used for estimating high-resolution (~1 km) SHPs through inverse modeling in the HYDRUS-1D software suit. The proposed method has the advantage of being independent of field data over the previously available methods (Pressure-plate lab experiments, in-situ soil moisture data, or regression equations) as all the methods require field sampling, which can be expensive, time-consuming and remote areas can be inaccessible. Even though the range set for inverse optimization can impact the SHP set obtained, point-based sampling is not possible for the regional scale. The dotty plot also shows the parameter sets that are possible to obtain but one needs to choose statistical parameters to minimize the uncertainty. The study shows that with the derivation of these SHPs, the simulation of the rootzone soil moisture is improved. The RZSM with this study is available at a scale of 1 km on a daily basis. Thus, in the context of previous studies, it can be seen that the estimated SHPs here are independent of in-situ soil moisture data, which itself are scarce or available in limited regions. Additionally, the estimated SHPs may perform better as compared to pedotransfer functions as they tend to be site-specific [22] and application to other regions results in the under or over-estimation of RZSM. Secondly, the derivation of SHPs is also independent of soil data collection, which again is not available at all places due to being time-consuming and expensive. The study, hence, provides a new method to improve the simulation of RZSM both spatially and temporally by improving the input dataset that has the effective SHPs. Although the study is limited by the fact that the soil profile has been treated as homogeneous, it is hypothesized that from the agricultural perspective or even shallow landslides, the soil layer is shallow and we can treat it as a homogeneous layer. Additionally, the results show that even though the soil profile is considered homogeneous, the results are comparable to the heterogeneous layer (Table 3) in the considered study area.

We would like to point out that the study is limited by the availability of the validation dataset. Additionally, the mismatch in the spatial resolution of the datasets further leads to uncertainty but the approach is promising. The future work would include looking at the derivation of these parameters based on the other available Earth observation datasets such as SMAP products and understanding the uncertainty based on the different products. It will also include deriving SHPs at a finer spatial resolution (30 m) and vertical resolution. This would entail further improvement of soil moisture simulation in deeper soil moisture layers.

6. Conclusions

A downscaling algorithm to downscale 25 km spatial resolution radiometer based AMSR-2 soil moisture to 1 km has been applied over a semi-arid region where the land is mostly used for agricultural activities. The obtained finer resolution surface soil moisture product has been used for inverse parameterization of SHPs and thus simulating RZSM through HYDRUS-1D. The performance of the algorithm has been validated temporally and spatially at 0.05 m, 0.20 m, and 0.50 m at a validation site; surface soil moisture simulation has been validated at 44 different locations in the Varanasi district of Uttar Pradesh, India.

In order to understand the performance of the spatial downscaling algorithm, a primary time series comparison has been carried out at one test site where the in-situ soil moisture is compared with AMSR-2 satellite-derived soil moisture (25 km) and downscaled soil moisture (1 km) for a period of six months from 1 January 2018 to 10 June 2018; the former has an *R*-value of 0.33 and the latter of 0.53. The temporal correlation between downscaled soil moisture product and HDS soil moisture is 0.704 whereas AMSR-2 has a significantly lower correlation (0.58) with the HDS soil moisture. The modeling of the water movement in the unsaturated soil based on Richard's Equation requires SHPs, which are important parameters in determining the retaining capacity of the soil. The SHPs play an important role in the partitioning of water to be infiltrated. These parameters are difficult to ascertain on a regional scale due to time-consuming and expensive field

experiments. In the current study, inverse optimization was conducted to obtain these parameters. However, the method requires the usage of the in-situ soil moisture dataset. Thus, six numerical experiments (*I-a*, *I-b*, *I-c*, *I-d*, *II-a* and *II-b*), were conducted to estimate the SHPs with various datasets that were considered as observed soil moisture. The soil moisture output of the *I-b* and *I-d* treatments distinctly stand out with markedly good correlation with the HDS data at three layers (surface, 20 cm and 50 cm). It was seen that the SHPs estimated using the downscaled soil moisture (*I-d* experiment) performed with similar efficiency as compared to SHPs estimated from the in-situ soil moisture data (*I-b* experiment) in simulating the soil moisture. The normalized nRMSE for the two treatments was 0.37 and 0.34, respectively. It is to be noted that the *I-a* treatment, which is based on soil texture and the *I-c* treatment, which uses coarser AMSR-2 soil moisture as an observed dataset have reduced performance among the four treatments. It was also noted that nRMSE for the treatment with the utilization of default SHPs (*I-a*) and AMSR-2 soil moisture (*I-c*) were found to be 0.50 and 0.43, respectively. This firstly illustrates the significance of site-specific derivation of SHPs for better soil moisture modeling. Secondly, the performance of the *I-d* treatment shows that downscaled AMSR-2 soil moisture can be utilized as the observed dataset in the absence of the in-situ soil moisture dataset. Even after considering the soil layer heterogenous, the default SHPs were not able to correlate as high as the *I-d* treatment for the calibration period. This shows that the downscaled AMSR-2 soil moisture information can be utilized to derive the parameters and improve the soil moisture simulations. *II-b* is found to be the best treatment among all six treatments considered in the present study. Although *II-b* outperformed all the treatments, its applicability is limited to the places where in-situ data are readily available. It was also seen that at the 44 sites, there was improvement in the mean NSE for the surface soil moisture simulation with the *I-d* treatment (0.50) as compared to the *I-a* treatment (0.10). Additionally, the study emphasizes that in the absence of in-situ soil moisture data, the inverse optimization scheme cannot be utilized. Thus, the methodology employed in this study provides an alternative source to be utilized as an observed dataset, which leads to an improved soil moisture simulation both at spatial and temporal scales. In conclusion, monitoring and assessment of surface soil moisture as well as RZSM is extremely significant for agriculture and many other applications; in reality, it is very difficult to obtain as the establishment and maintenance of soil moisture observation networks have huge costs. Thus, the present study is significant as the method proposed for estimating the SHPs and simulating high-resolution soil moisture is based entirely on satellite-derived datasets.

Conflicts of Interest: The authors have no conflicts of interest to declare. All co-authors have seen and agreed with the contents of the manuscript and there is no financial interest to report. We certify that the submission is original work and is not under review at any other publication.

References

1. Colliander, A.; Fisher, J.B.; Halverson, G.; Merlin, O.; Misra, S.; Bindlish, R.; Jackson, T.J.; Yueh, S. Spatial downscaling of SMAP soil moisture using MODIS land surface temperature and NDVI during SMAPVEX15. *IEEE Geosci. Remote Sens. Lett.* **2017**, *14*, 2107–2111. [CrossRef]
2. Peng, J.; Loew, A.; Merlin, O.; Verhoest, N.E. A review of spatial downscaling of satellite remotely sensed soil moisture. *Rev. Geophys.* **2017**, *55*, 341–366. [CrossRef]
3. Vereecken, H.; Huisman, J.; Pachepsky, Y.; Montzka, C.; Van Der Kruk, J.; Bogena, H.; Weihermüller, L.; Herbst, M.; Martinez, G.; Vanderborght, J. On the spatio-temporal dynamics of soil moisture at the field scale. *J. Hydrol.* **2014**, *516*, 76–96. [CrossRef]
4. Petropoulos, G.; Carlson, T.; Wooster, M.; Islam, S. A review of Ts/VI remote sensing based methods for the retrieval of land surface energy fluxes and soil surface moisture. *Prog. Phys. Geogr.* **2009**, *33*, 224–250. [CrossRef]
5. Bastiaanssen, W.G.; Molden, D.J.; Makin, I.W. Remote sensing for irrigated agriculture: Examples from research and possible applications. *Agric. Water Manag.* **2000**, *46*, 137–155. [CrossRef]
6. Douville, H.; Viterbo, P.; Mahfouf, J.-F.; Beljaars, A.C. Evaluation of the optimum interpolation and nudging techniques for soil moisture analysis using FIFE data. *Mon. Weather. Rev.* **2000**, *128*, 1733–1756. [CrossRef]
7. Nemani, R.; Hashimoto, H.; Votava, P.; Melton, F.; Wang, W.; Michaelis, A.; Mutch, L.; Milesi, C.; Hiatt, S.; White, M. Monitoring and forecasting ecosystem dynamics using the Terrestrial Observation and Prediction System (TOPS). *Remote Sens. Environ.* **2009**, *113*, 1497–1509. [CrossRef]
8. Reichstein, M.; Rey, A.; Freibauer, A.; Tenhunen, J.; Valentini, R.; Banza, J.; Casals, P.; Cheng, Y.; Grünzweig, J.M.; Irvine, J. Modeling temporal and large-scale spatial variability of soil respiration from soil water availability, temperature and vegetation productivity indices. *Glob. Biogeochem. Cycles* **2003**, *17*, 1104. [CrossRef]
9. Esit, M.; Kumar, S.; Pandey, A.; Lawrence, D.M.; Rangwala, I.; Yeager, S. Seasonal to multi-year soil moisture drought forecasting. *NPJ Clim. Atmos. Sci.* **2021**, *4*, 16. [CrossRef]
10. Hu, W.; Xu, Q.; Wang, G.; Van Asch, T.; Hicher, P.-Y. Sensitivity of the initiation of debris flow to initial soil moisture. *Landslides* **2015**, *12*, 1139–1145. [CrossRef]
11. Marino, P.; Peres, D.J.; Cancelliere, A.; Greco, R.; Bogaard, T.A. Soil moisture information can improve shallow landslide forecasting using the hydrometeorological threshold approach. *Landslides* **2020**, *17*, 2041–2054. [CrossRef]
12. Wasko, C.; Nathan, R. Influence of changes in rainfall and soil moisture on trends in flooding. *J. Hydrol.* **2019**, *575*, 432–441. [CrossRef]
13. Zeri, M.; Williams, K.; Cunha, A.P.M.; Cunha-Zeri, G.; Vianna, M.S.; Blyth, E.M.; Marthews, T.R.; Hayman, G.D.; Costa, J.M.; Marengo, J.A. Importance of including soil moisture in drought monitoring over the Brazilian semiarid region: An evaluation using the JULES model, in situ observations, and remote sensing. *Clim. Resil. Sustain.* **2022**, *1*, e7. [CrossRef]
14. Zhao, Y.; Yang, H.; Wei, F. Soil moisture retrieval with remote sensing images for debris flow forecast in humid regions. *Monit. Simul. Prev. Remediat. Dense Debris Flows III* **2010**, *67*, 11189.
15. Loew, A. Impact of surface heterogeneity on surface soil moisture retrievals from passive microwave data at the regional scale: The Upper Danube case. *Remote Sens. Environ.* **2008**, *112*, 231–248. [CrossRef]
16. Jackson, T.J.; Hsu, A.Y.; O'Neill, P.E. Surface soil moisture retrieval and mapping using high-frequency microwave satellite observations in the Southern Great Plains. *J. Hydrometeorol.* **2002**, *3*, 688–699. [CrossRef]
17. Wu, X.; Walker, J.P.; Rüdiger, C.; Panciera, R. Effect of land-cover type on the SMAP active/passive soil moisture downscaling algorithm performance. *IEEE Geosci. Remote Sens. Lett.* **2014**, *12*, 846–850.
18. Wagner, W.; Naeimi, V.; Scipal, K.; de Jeu, R.; Martínez-Fernández, J. Soil moisture from operational meteorological satellites. *Hydrogeol. J.* **2007**, *15*, 121–131. [CrossRef]
19. Mishra, V.; Ellenburg, W.L.; Griffin, R.E.; Mecikalski, J.R.; Cruise, J.F.; Hain, C.R.; Anderson, M.C. An initial assessment of a SMAP soil moisture disaggregation scheme using TIR surface evaporation data over the continental United States. *Int. J. Appl. Earth Obs. Geoinf.* **2018**, *68*, 92–104. [CrossRef]

20. Das, N.N.; Entekhabi, D.; Dunbar, S.; Kim, S.-B.; Yueh, S.; Colliander, A.; O'Neill, P.; Jackson, T.J.; Jagdhuber, T.; Chen, F. *SMAP/Sentinel-1 L2 Radiometer/Radar 30-Second Scene 3 km EASE-Grid Soil Moisture-Global*; NASA National Snow and Ice Data Center Distributed Active Archive Center: Boulder, CO, USA, 2019.

21. Wentz, F.; Meissner, T.; Gentemann, C.; Hilburn, K.; Scott, J. *Remote Sensing Systems GCOM-W1 AMSR2 Daily Environmental Suite on 0.25 Deg Grid*, version 7.2; Remote Sensing Systems: Santa Rosa, CA, USA, 2014.

22. Garg, N.; Gupta, M. Assessment of improved soil hydraulic parameters for soil water content simulation and irrigation scheduling. *Irrig. Sci.* **2015**, *33*, 247–264. [CrossRef]

23. Dash, S.K.; Sinha, R. A Comprehensive Evaluation of Gridded L-, C-, and X-Band Microwave Soil Moisture Product over the CZO in the Central Ganga Plains, India. *Remote Sens.* **2022**, *14*, 1629. [CrossRef]

24. Merlin, O.; Al Bitar, A.; Walker, J.P.; Kerr, Y. An improved algorithm for disaggregating microwave-derived soil moisture based on red, near-infrared and thermal-infrared data. *Remote Sens. Environ.* **2010**, *114*, 2305–2316. [CrossRef]

25. Piles, M.; Camps, A.; Vall-Llossera, M.; Corbella, I.; Panciera, R.; Rudiger, C.; Kerr, Y.H.; Walker, J. Downscaling SMOS-derived soil moisture using MODIS visible/infrared data. *IEEE Trans. Geosci. Remote Sens.* **2011**, *49*, 3156–3166. [CrossRef]

26. Merlin, O.; Walker, J.P.; Chehbouni, A.; Kerr, Y. Towards deterministic downscaling of SMOS soil moisture using MODIS derived soil evaporative efficiency. *Remote Sens. Environ.* **2008**, *112*, 3935–3946. [CrossRef]

27. Merlin, O.; Chehbouni, A.; Walker, J.P.; Panciera, R.; Kerr, Y.H. A simple method to disaggregate passive microwave-based soil moisture. *IEEE Trans. Geosci. Remote Sens.* **2008**, *46*, 786–796. [CrossRef]

28. Merlin, O.; Al Bitar, A.; Walker, J.P.; Kerr, Y. A sequential model for disaggregating near-surface soil moisture observations using multi-resolution thermal sensors. *Remote Sens. Environ.* **2009**, *113*, 2275–2284. [CrossRef]

29. Šimůnek, J.; van Genuchten, M.T.; Šejna, M. Development and applications of the HYDRUS and STANMOD software packages and related codes. *Vadose Zone J.* **2008**, *7*, 587–600. [CrossRef]

30. Kottek, M.; Grieser, J.; Beck, C.; Rudolf, B.; Rubel, F. World Map of the Köppen-Geiger climate classification updated. *Meteorol. Z.* **2006**, *15*, 259–263. [CrossRef]

31. Varanasi Mines Officer. *District Survey Report for Planning and Execution of Minor Mineral Excavation*; National Informatics Center Varanasi: Varanasi, India, 2020.

32. Nistor, M.M.; Rai, P.K.; Dugesar, V.; Mishra, V.N.; Singh, P.; Arora, A.; Kumra, V.K.; Carebia, I.A. Climate change effect on water resources in Varanasi district, India. *Meteorol. Appl.* **2020**, *27*, e1863. [CrossRef]

33. Lehner, B.; Verdin, K.; Jarvis, A. New global hydrography derived from spaceborne elevation data. *EOS Trans. Am. Geophys. Union* **2008**, *89*, 93–94. [CrossRef]

34. Gruber, A.; Dorigo, W.A.; Zwieback, S.; Xaver, A.; Wagner, W. Characterizing coarse-scale representativeness of in situ soil moisture measurements from the International Soil Moisture Network. *Vadose Zone J.* **2013**, *12*, vzj2012.0170. [CrossRef]

35. Jabro, J.; Stevens, W.; Iversen, W. Field performance of three real-time moisture sensors in sandy loam and clay loam soils. *Arch. Agron. Soil Sci.* **2018**, *64*, 930–938. [CrossRef]

36. Sharma, J.; Prasad, R.; Srivastava, P.K.; Singh, S.K.; Yadav, S.A.; Yadav, V.P. Roughness characterization and disaggregation of coarse resolution SMAP soil moisture using single-channel algorithm. *J. Appl. Remote Sens.* **2021**, *15*, 014514. [CrossRef]

37. Wan, Z.; Hook, S.; Hulley, G. *MOD11A1 MODIS/Terra Land Surface Temperature and the Emissivity Daily L3 Global 1km SIN Grid*; NASA LP DAAC: Sioux Falls, SD, USA, 2015.

38. Didan, K. *MOD13A2 MODIS/Terra Vegetation Indices 16-Day L3 Global 1km SIN Grid V006*; NASA LP DAAC: Sioux Falls, SD, USA, 2015; No. 10.

39. Myneni, R.; Knyazikhin, Y.; Park, T. *MOD15A2H MODIS/Terra leaf area Index/FPAR 8-Day L4 Global 500m SIN grid V006*; NASA LP DAAC: Sioux Falls, SD, USA, 2015.

40. Boschetti, L.; Vermote, E.; Wolfe, R. *MODTBGA MODIS/Terra Thermal Bands Daily L2G-lite Global 1km SIN grid V006*; NASA LP DAAC: Sioux Falls, SD, USA, 2015.

41. Owe, M.; de Jeu, R.; Walker, J. A methodology for surface soil moisture and vegetation optical depth retrieval using the microwave polarization difference index. *IEEE Trans. Geosci. Remote Sens.* **2001**, *39*, 1643–1654. [CrossRef]

42. Dorigo, W.; Wagner, W.; Hohensinn, R.; Hahn, S.; Paulik, C.; Xaver, A.; Gruber, A.; Drusch, M.; Mecklenburg, S.; van Oevelen, P. The International Soil Moisture Network: A data hosting facility for global in situ soil moisture measurements. *Hydrol. Earth Syst. Sci.* **2011**, *15*, 1675–1698. [CrossRef]

43. Tian, Y.; Peters-Lidard, C.D.; Kumar, S.V.; Geiger, J.; Houser, P.R.; Eastman, J.L.; Dirmeyer, P.; Doty, B.; Adams, J. High-performance land surface modeling with a Linux cluster. *Comput. Geosci.* **2008**, *34*, 1492–1504. [CrossRef]

44. Stackhouse, P.; Zhang, T.; Westberg, D.; Barnett, A.J.; Bristow, T.; Macpherson, B.; Hoell, J.M. *POWER Release 8.0. 1 (with GIS applications) Methodology (Data Parameters, Sources, & Validation)*; NASA Langley Research Centre: Hampton, VA, USA, 2018.

45. Li, Z.-L.; Tang, R.; Wan, Z.; Bi, Y.; Zhou, C.; Tang, B.; Yan, G.; Zhang, X. A review of current methodologies for regional evapotranspiration estimation from remotely sensed data. *Sensors* **2009**, *9*, 3801–3853. [CrossRef]

46. Goetz, S. Multi-sensor analysis of NDVI, surface temperature and biophysical variables at a mixed grassland site. *Int. J. Remote Sens.* **1997**, *18*, 71–94. [CrossRef]

47. Nemani, R.; Pierce, L.; Running, S.; Goward, S. Developing satellite-derived estimates of surface moisture status. *J. Appl. Meteorol. Climatol.* **1993**, *32*, 548–557. [CrossRef]

48. Rahimzadeh-Bajgiran, P.; Berg, A. Soil moisture retrievals using optical/TIR methods. In *Satellite Soil Moisture Retrieval*; Elsevier: Amsterdam, The Netherlands, 2016; pp. 47–72.
49. Team, R.C. *R: A Language and Environment for Statistical Computing*; RC Team: Vienna, Austria, 2013.
50. Mattiuzzi, M.; Detsch, F. *MODIS: Acquisition and Processing of MODIS Products*; RC Team: Vienna, Austria, 2016.
51. Atzberger, C.; Eilers, P.H. A time series for monitoring vegetation activity and phenology at 10-daily time steps covering large parts of South America. *Int. J. Digit. Earth* **2011**, *4*, 365–386. [CrossRef]
52. Pablos, M.; González-Zamora, Á.; Sánchez, N.; Martínez-Fernández, J. Assessment of root zone soil moisture estimations from SMAP, SMOS and MODIS observations. *Remote Sens.* **2018**, *10*, 981. [CrossRef]
53. Gupta, M.; Garg, N.; Joshi, H.; Sharma, M. Persistence and mobility of 2, 4-D in unsaturated soil zone under winter wheat crop in sub-tropical region of India. *Agric. Ecosyst. Environ.* **2012**, *146*, 60–72. [CrossRef]
54. Allen, R.G.; Pereira, L.S.; Raes, D.; Smith, M. *Crop Evapotranspiration-Guidelines for Computing Crop Water Requirements*; FAO Irrigation and Drainage Paper 56; FAO: Rome, Italy, 1998; Volume 300, p. D05109.
55. Van Genuchten, M.T. A closed-form equation for predicting the hydraulic conductivity of unsaturated soils. *Soil Sci. Soc. Am. J.* **1980**, *44*, 892–898. [CrossRef]
56. Mualem, Y. A new model for predicting the hydraulic conductivity of unsaturated porous media. *Water Resour. Res.* **1976**, *12*, 513–522. [CrossRef]
57. Srivastava, P.K.; Petropoulos, G.P.; Prasad, R.; Triantakonstantis, D. Random Forests with Bagging and Genetic Algorithms Coupled with Least Trimmed Squares Regression for Soil Moisture Deficit Using SMOS Satellite Soil Moisture. *ISPRS Int. J. Geo-Inf.* **2021**, *10*, 507. [CrossRef]
58. Srivastava, P.K.; Han, D.; Yaduvanshi, A.; Petropoulos, G.P.; Singh, S.K.; Mall, R.K.; Prasad, R. Reference evapotranspiration retrievals from a mesoscale model based weather variables for soil moisture deficit estimation. *Sustainability* **2017**, *9*, 1971. [CrossRef]